

Drew University College of the Liberal Arts

**A Mechanistic and Kinetic Comparison of the Reactivity of
Volatile Organic Compounds on Mineral Dusts**

Baldwin Honors Thesis in Chemistry by
Madeline Rose Lederer

May 2016

Committee:

Dr. Ryan Hinrichs

Dr. Maryann Pearsall

Dr. Bjorg Larson

Dr. Bai Di

Acknowledgements

First and foremost, I would like to thank my research advisor and mentor Dr. Hinrichs. He has offered guidance and support throughout my time at Drew, and without him I never could have completed this project. His passion for research and teaching have inspired me and made me love this project. I would also like to thank my committee for their support. First, Dr. Pearsall who has offered me so many comments and suggestions, who convinced me after two years to pursue a major in Chemistry, and who has advised me for the last four years. Next, Dr. Bjorg Larson who has been supportive of my work from the beginning. I would also like to thank my committee chair Dr. Bai Di who has been so helpful in providing an outside opinion on my work and helping me to meet deadlines and organize this project. I would like to thank my friends who spent a summer doing research with me as part of the Drew Summer Science Institute and who have been with me throughout the entire writing process. I would like to acknowledge my fellow researchers Allison Staniec, who's project I adopted, and Zoe Coates Fuentes who assisted me for the summer and without whom this thesis would never have reached the scale it has. Finally, I need to thank the Drew University Chemistry Department, The National Science Foundation, and the Baldwin Honors Program for financial support and allowing me the unique experience to pursue research during my undergraduate career.

Abstract

Laboratory models of atmospheric systems have attempted to account for causes and effects of major dust events in recent decades, but these models lack many key components of actual dust storms. Elemental analysis of atmospheric dust places silicon and aluminum as the most abundant elements in many storms, leading many to assume that the oxides of these elements – SiO_2 and Al_2O_3 – accurately reflect mineral aerosol surfaces. More detailed field studies indicate that aluminosilicate clays are actually the prevalent surfaces in the atmosphere, though these clays are not widely studied in laboratory models. This work aims to assess the current assumption that Al_2O_3 and SiO_2 reactivity can be used to model aluminosilicate clay aerosols by systematically collecting data on kinetics, product formation, and particle size. Limonene was used as a model volatile organic compound and found to produce a variety of secondary organic products, as displayed in the figure below, that will be discussed mechanistically with their relation to the reactive Brønsted acid, Lewis acid, and Redox sites on each dust sample. Our results indicate that clay reactivity differs greatly from that of Al_2O_3 due to significant differences in surface structure. Nitric acid was also shown to increase reactive uptake of limonene on mineral surfaces by factors of 6.21 to 16.4, with the greatest value of γ in the reaction of nitric acid coated kaolinite: $3.656 \cdot 10^{-8}$.

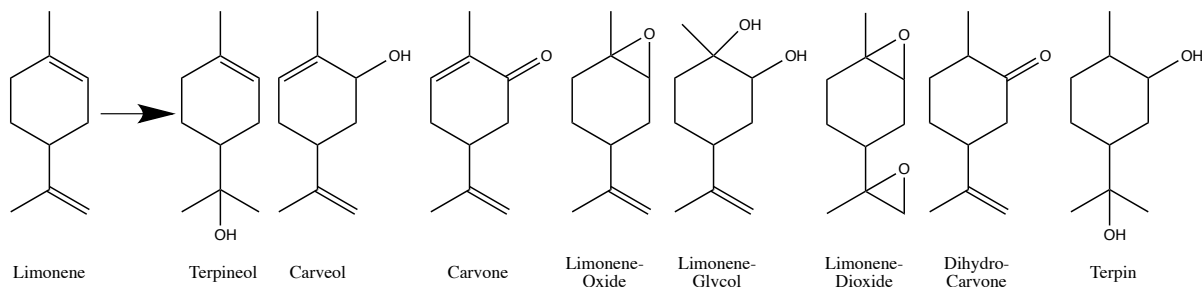


Table of Contents

Abstract	3
Glossary	5
Chapter 1: Introduction	7
1.1 Dust Storm Composition and the Oxide Based Approach	13
1.2 The Surface Structure of Mineral Dusts	16
1.3 Reactions of Mineral Dust with Trace Atmospheric Gases	19
1.4 Goals of the Current Study	24
Chapter 2: Materials and Methods	27
2.1 Gas Preparation	28
2.2 Reaction Monitoring	29
2.3 Dust Preparation	30
2.4 Product Identification	32
2.5 Surface Area and Particle Size Profiling	34
2.6 Reactive Uptake Calculation	35
Chapter 3: Products and Mechanisms of Product Formation of the Reaction of Limonene on Mineral Dusts	36
3.1 Mechanistic Descriptions of Each Observed Product	40
3.2 A Discussion of the Effects of Mineral Dust Structure on Product Formation	51
Chapter 4: A Kinetic Comparison of Mineral Dusts	63
4.1 Kinetics of Oxides	65
4.2 Kinetics of Clays	69
4.3 Kinetics of a Mixed Dust	72
4.4 Effects of Acid on Particle Size	74
Chapter 5: Conclusions	81
5.1 A Summary of the Results	81
5.2 Recommendations for Ongoing Research	87
Bibliography	89

Glossary (Based off of the IPCC Fourth Annual Report- Annex I)

Aluminosilicate Clay: Dust composed of aluminum and silicon mineral centers bonded to oxygen. They usually form 2 or 3 layers of octahedral aluminum and tetrahedral silica alternating. They may have ion substitutions (K, Mg, Ca, Na) within the lattice or between sheets. This paper discusses kaolinite, illite, and Ca-rich montmorillonite (see Figure 5).

Anthropogenic: Gases that are emitted by human activities, such as pollution from industry.

BET: Brunauer–Emmett–Teller theory which explains the adsorption of gases onto solids to determine surface area and pore size of the solid.

Biogenic: Gases that come from natural sources, such as emission from vegetation.

Carbonate clay: Dust composed of one or more elements as mineral centers bonded to CO₃ groups. The most common example is CaCO₃, or calcite (see Figure 4).

Clay: Dust composed of multiple mineral centers with oxygen within the lattice. Some oxygen are also bonded to hydrogen, primarily at edge sites. Types of clays discussed include carbonates and aluminosilicates.

Cloud Condensation Nuclei: (CCN) Small atmospheric particles that allow water vapor to condense and form cloud droplets.

DRIFTS: Diffuse Reflectance Infrared Fourier Transform Spectroscopy. A type of IR spectroscopy that monitors the light scattering on the surface of a solid.

Endo-unsaturation: A double bond located inside the cyclohexane ring of limonene.

Exo-unsaturation: The double bond located on the isopropyl side chain of limonene.

Greenhouse Gases: (GHGs) Atmospheric gases that absorb thermal infrared radiation and thus cause warming by positive radiative forcing.

Monoterpenes: Compounds derived from two isoprene subunits.

Oxide Dust: A dust composed solely of one element, such as Si or Al, and oxygen. The surfaces may be hydrated and contain some hydrogen at edges, but the primary crystal structure is only mineral centers and oxygen. See Figure 3.

Radiative Forcing: The way in which gases affect the energy balance between solar radiation entering the atmosphere and infrared radiation that is able to leave. Some gases trap infrared radiation, which causes warming, so they have a positive radiative forcing value (Watts/m²).

Reactive Uptake Coefficient (γ): A measure of the reactivity of a surface with a gaseous particle.

Secondary Organic Aerosol: (SOA) Products of reactions with VOCs. These pollutants are usually less volatile than their predecessors and are gaseous.

Secondary Organic Matter: (SOM) Proposed products of reactions with VOCs on solid atmospheric particles. These products are less volatile than their VOC predecessors and thus remain adsorbed onto solid particles.

TIC: Total Ion Chromatogram. In this study, these are the digital results of UV absorption of different compounds as they elute from a gas chromatography column.

Trace Gases: Atmospheric gases that occur in lower concentrations compared to major species such as N_2 , O_2 , CO_2 , CH_4 , etc. Trace gases discussed in this paper include isoprene and monoterpenes.

Volatile: Substances that easily become gaseous and evaporate quickly

Volatile Organic Compounds: (VOCs) Organic compounds that evaporate easily and thus exist in the atmosphere as gases that can potentially react with other atmospheric species.

Chapter 1: Introduction

Mineral dust is a ubiquitous component of the atmosphere. Deriving from the soil, these particulates are lifted by the wind and transported around the world as major dust storms or miniscule particles in clouds. Growing numbers of satellites monitoring changes in weather patterns and the global environment have facilitated advanced study of the atmosphere. By monitoring changes in temperature, cloud formation, and other weather patterns over long periods of time, we have been able to see trends and better predict changes in climate. Through the new information on climatic patterns, questions have emerged about how and why we experience climate change and how human activities play a part. Atmospheric research exploded forth from these questions, and with the constant improvements in modeling and monitoring technology, these fields will continue to grow.

One of these burgeoning fields has been the study of atmospheric chemistry. Modeling the reactions that occur between gases or vapors that organisms release into the air with the naturally occurring components of our atmosphere has been a major aspect of understanding climate change. A major question previously left unanswered was the source and effects of the North American Dust Bowl during the mid 1930s. Coupled with the Great Depression, the Dust Bowl left western prairies without topsoil for crops and in a major drought, while the farmers and their families were forced out of dust-choked homes into coastal cities¹. Where had this drought come from? And what happened to all of the dust? Recent studies have linked plant loss and human activity to global temperature increases during this period and the inability of clouds to form and precipitate². The expansion of studies on global warming and human exacerbation of change in radiative forcing (**Figure 1**) have allowed researchers to gain significant insight into many of the chemical processes occurring in the atmosphere. As shown

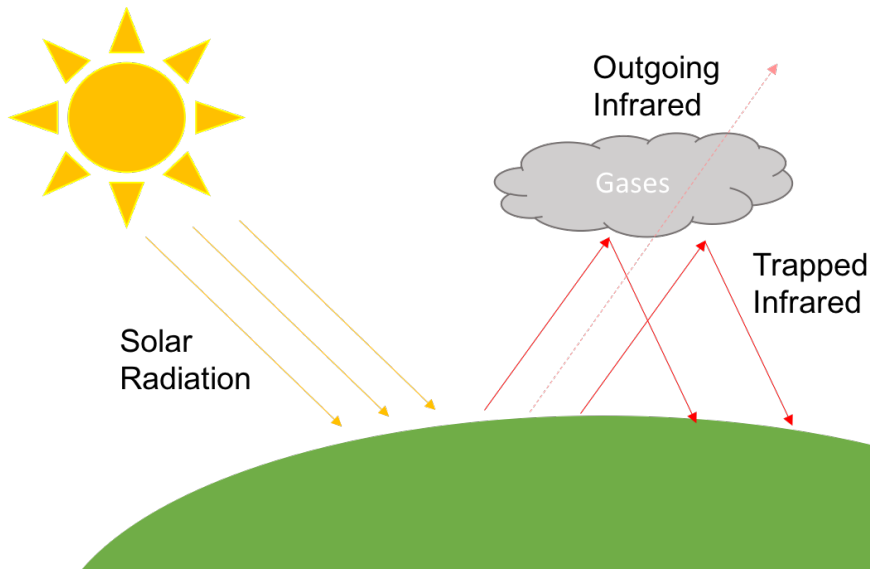


Figure 1: Radiative forcing is a measure of trapped infrared radiation by atmospheric gases. It is defined as the difference between incoming solar radiation and outgoing infrared, which creates an energy imbalance³, and thus either heating or cooling.

in **Figure 2**, one of the most extensively studied classes of atmospheric constituents is greenhouse gases. There is a high level of scientific understanding of greenhouse gases (GHGs), and they have a net warming impact due to positive radiative forcing. **Figure 2** also demonstrates that in the boom of research on GHGs, many other classes of atmospheric gases

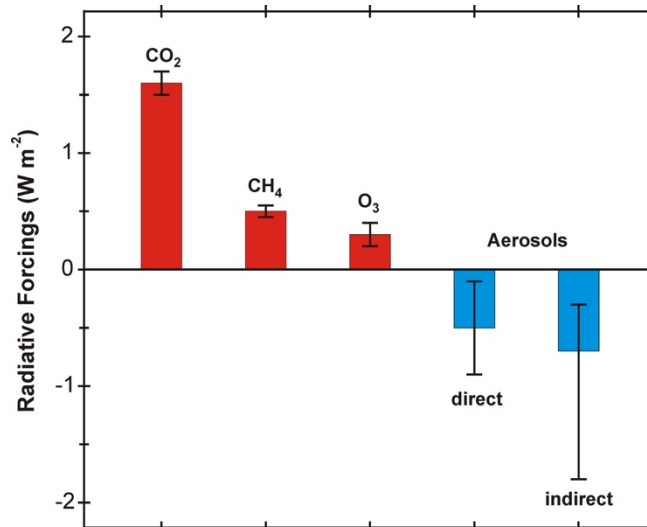


Figure 2: Level of scientific understanding of different atmospheric species, and their known effects. Bars represent the warming and cooling effects of different atmospheric particles, and they are sorted by level of scientific understanding, with greenhouse gases and ozone being most well studied.

and particles were largely ignored. Noticeably, aerosols, both their direct and indirect effects, are generally cooling and are not well understood, as demonstrated by the large error bars. The large error and lack of understanding of these two factors still leaves a large gap in comprehending the effects of the Dust Bowl. More study of mineral dusts and aerosols is needed to create a complete description of our atmosphere.

In addition to the western United States, deserts around the world are the major sources of mineral dust in the air. Estimations put mineral dust emissions between 1000 and 3000 Tg per year⁴, and they have been implicated in total atmospheric warming due to the different radiative effects of absorbing and scattering⁵. The EPA calculated that GHG emissions in 2011 reached 6,702.3 Tg in CO₂ equivalents⁶, therefore mineral dusts are emitted at high enough levels to have comparable relevance with a number of different GHGs. Mass is not the only important factor in measuring radiative effects; the impact per particle is an important consideration in these calculations. Particles that are more reactive, but weigh less, can have a greater effect than particles with a large mass but low reactivity. We have studied a variety of different size dust particles kinetically to account for different reactivity per particle. Dust can be eroded from rock surfaces or from soil due to the wind, and the particles are lifted into clouds. Large scale events like those in Asia, the Mediterranean, and Saharan Africa are the most widely studied as they are reliable sources of large dust storms annually⁷⁻⁹. Eroded dust particles come in a variety of masses and sizes, but only the small, light particles travel long distances and remain relevant in determining radiative forcing.

Besides the warming and cooling due to the aging of dust particles, altered ice nucleation and erosion are important considerations for the relevance of mineral aerosol study. Many studies show mineral dust acting as cloud condensation nuclei (CCN)¹⁰. Dusts can

increase the number of CCN and ice-like water in clouds when dissolved in the water droplets¹¹, so ice nuclei may be forming more readily in warmer conditions that would usually not favor them. Clays also increase the temperature at which the ice nuclei can form, which has an overall atmospheric cooling effect¹². After mineral dusts react, a process often referred to as “aging”, they can have altered effects on the atmosphere. The forcing varies before and after aging of dusts, indicating that the surfaces can transition from cooling to warming effects, or move towards and away from extremes dependent on the scattering or absorbing properties of the dust. Coating of mineral dusts with organics can decrease their ability to act as CCN¹¹. Within these changes lie additional variables in determining the forcing due to the composition of the dusts. Oxide dusts, like Al₂O₃ or Fe₂O₃, have a different radiative forcing than clays, such as kaolinite or smectite, due to the different scattering properties¹³. It is clear that understanding mineral dusts is a complex undertaking due to the wide variability in every aspect of composition and effects.

Major classes of dust particles are oxides, carbonates, and clays, and each have unique properties. Oxides are the most commonly studied minerals and include iron oxide (Fe₂O₃), alumina (Al₂O₃), and quartz/silica (SiO₂). **Figure 3** shows the crystal structures for alumina and quartz, the two oxides studied in this thesis. They are classified as oxides purely because they contain no other elements besides the mineral centers surrounded by oxygen. They can take on different configurations, but as will be described, the minor structural differences within a type of oxide do not significantly affect reactivity. Oxides are often hydroxylated in hydrated environments, such as the atmospherically relevant reaction conditions in this work, but it is important to note that the crystal structures displayed are not hydroxylated, so none of the reactive –OH groups are shown.

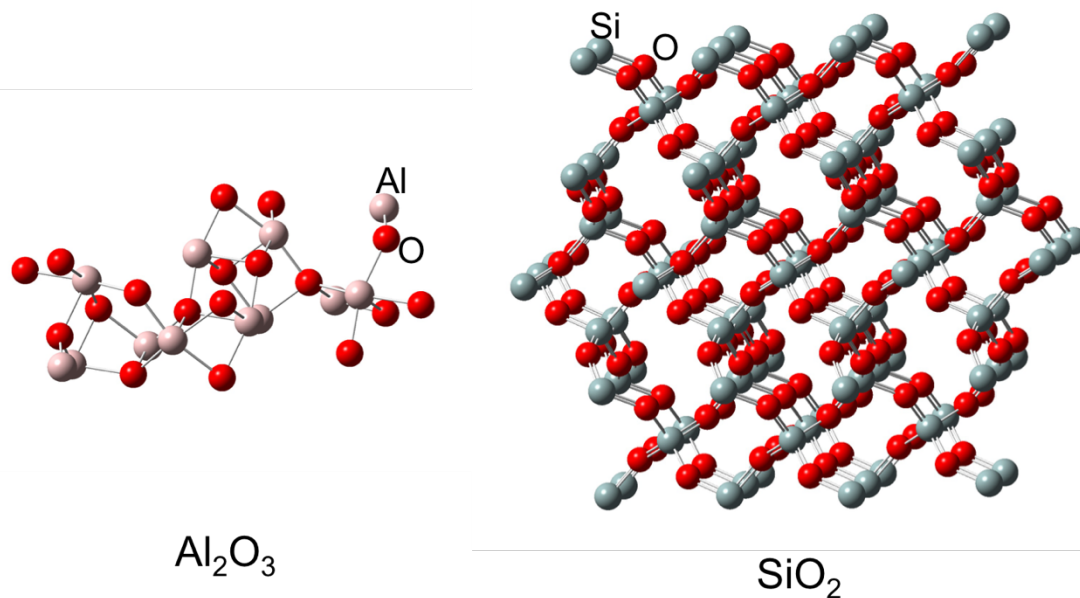


Figure 3: Gaussian structures of aluminum-oxide (alumina) and silicon-oxide (silica/quartz). Both are shown as dehydrated structures. Al is pink, Si is grey, and O is red.

A second particle class is the carbonates, where the most commonly studied and found is Calcite (CaCO_3) (**Figure 4**). Calcite was tested but it did not react in our experimental conditions, thus is it not described in detail in this thesis.

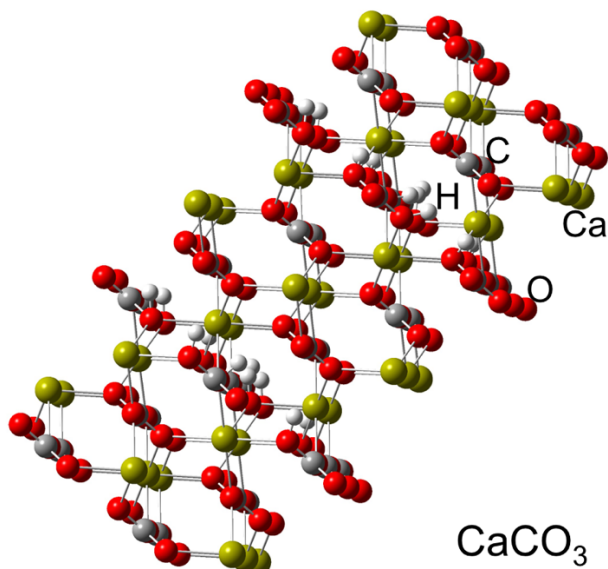


Figure 4: Gaussian structure of calcite, one of the carbonate clays. This structure is hydrated; Ca is yellow, C is grey, O is red, and H is white.

Clays are a much broader class of mineral particles. They are generally composed of one or more mineral/metal elements as a center, and either oxygen or hydroxide. Aluminosilicates are one of the other major classes of clays, and they are made up of aluminum, silicon, oxygen, and occasional metal ions. **Figure 5** shows two of the aluminosilicates studied in this thesis: kaolinite ($\text{Al}_2\text{Si}_2\text{O}_5(\text{OH})_4$) and montmorillonite ($(\text{Ca}_{.27}\text{Na}_{.04}\text{K}_{.01})[\text{Al}_{2.41}\text{Fe(III)}_{.09}\text{Mg}_{.71}\text{Ti}_{.03}][\text{Si}_8]\text{O}_{20}(\text{OH})_4$). Many clays, such as montmorillonite, have ionic substitutions within and between layers as shown in **Figure 5**. Because clays form layers, instead of large crystal structures like the oxides, water and other molecules can also move between the layers.

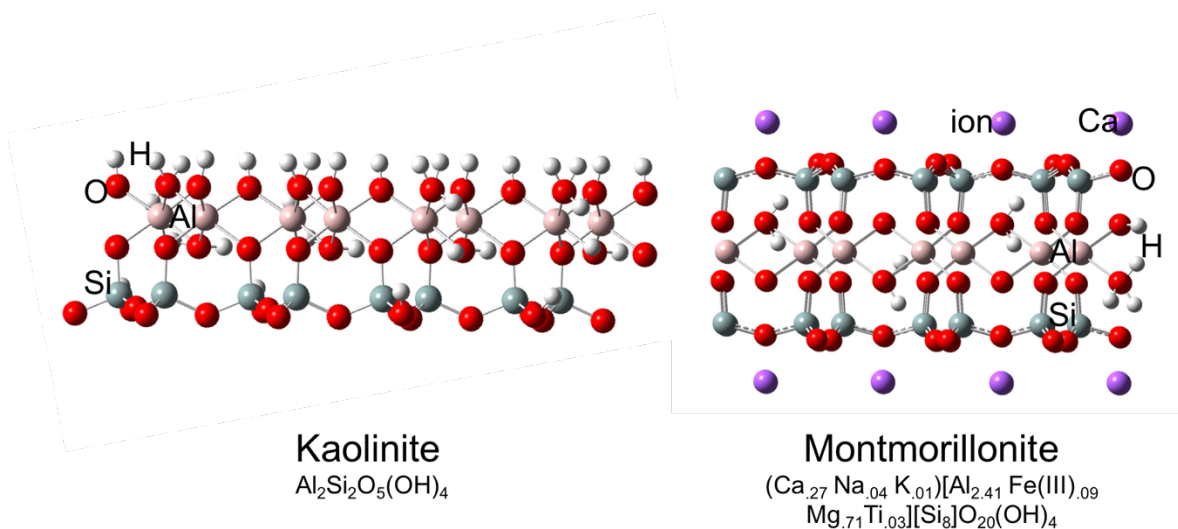


Figure 5: Gaussian structures of kaolinite and montmorillonite with only one layer shown. Both structures are hydrated; Si is grey, Al is pink, O is red, H is white, ions are purple- in our samples the ions are likely Ca.

Currently, mineral dusts can be characterized by their size, their composition or structure, and their reactivity. The composition and structure of particles is potentially the most important characteristic due widely to the variability in structures, as shown above. Elemental ratios and particle sizes can give a rough estimate of dust types present, but it is essential to understand the causes for the altered composition, reactivity, and size. Our study aims to fill the gaps in our knowledge of these characteristics. While some data exists on elemental

composition, there is a general lack of knowledge on the reactivity of mineral aerosols. It is our hope that optimization of modeling studies to focus on clays, not oxides, will help promote more accurate representations of mineral aerosol chemistry and help account for some of the global SOA production not described in other works.

1.1 Dust Storm Composition and the Oxide Based Approach

It is important to note that not all dust storms are created equal. Through the 1990s, the majority of atmospheric models represented dusts as homogenous mixtures of minerals with one refractive index and radiative impact throughout¹³, which created the basis for many simplified models used in labs today. In studying the large number of global dust storms, different particles have been identified in certain dust storms based on the soil composition of the source, thus disproving models of homogeneously composed dusts. Studies of dust clouds using X-ray diffraction and infrared have expanded our knowledge on the components of these storms and their lifetimes⁷⁻⁹. Collecting dust samples and monitoring them from satellites has begun to provide more data on their sources, compositions and trajectories. In the source locations of many dust storms, much of the clay and silt fractions of soil are composed of illite ($K_{.65}Al_2[Al_{.65}Si_{3.35}O_{10}](OH)_2$), kaolinite ($Al_2Si_2O_5(OH)_4$), quartz (SiO_2), and smectites- which include montmorillonite ($(Ca_{.27} Na_{.04} K_{.01})[Al_{2.41}Fe(III)_{.09} Mg_{.71}Ti_{.03}][Si_8]O_{20}(OH)_4$)¹³. African dust storms depositing over Spain and the Mediterranean have a red color, due to the high iron content, but smectite, illite, and quartz were identified as the predominant minerals in these storms⁷. In storms travelling across the Atlantic Ocean, researchers have the ability to monitor storms at different time points due to the long period and range of transport. In these storms, illite begins as the dominant mineral, but over time the ratios of illite to kaolinite decrease as transport time goes from hours to days⁹. By performing more in depth profiling of dust storms,

specific elements can be identified as characteristic of different soils. In a review by Usher et al. regional elemental compositions were compared, with Si remaining the most dominant element in all tested locations, followed closely by Al and Ca (**Figure 6**) based on a prior study by Wedepohl¹⁴. Interestingly, data on the relationship between silicon and aluminum as they occur in aerosols has shown that silicon can occur without being linked to any other major element, but aluminum never occurs without silicon present⁸. This observation agrees with the abundance of aluminosilicate clays that make up the mineral portion of atmospheric aerosols, and it indicates that pure mineral oxides, other than silicon oxide, may not be as atmospherically relevant as is often assumed.

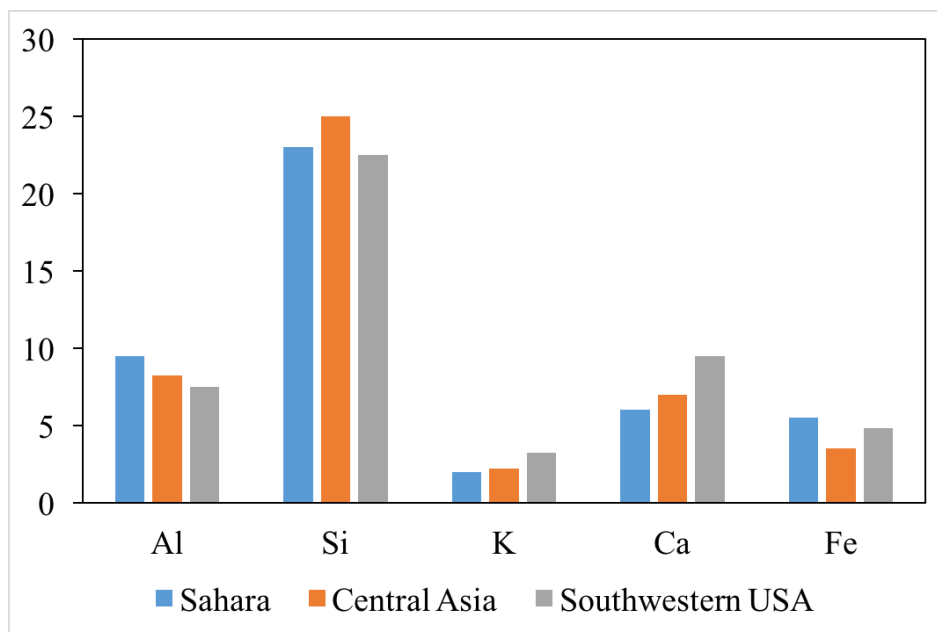


Figure 6: Relative elemental composition of dust samples by region. The data source for this figure was a figure by Usher et al.

Many studies have used elemental composition of dust storms as the primary mechanism of characterization of mineral aerosols, in opposition to our model. This focus on elements has produced heavily oxide favored models, which cause elemental oxides such as Al_2O_3 , Fe_2O_3 , Fe_3O_4 , SiO_2 , and TiO_2 to be the most widely studied mineral surfaces⁴ in

laboratory experiments. Our data and the previously discussed storm composition studies suggests that only silicon oxide and mixed elemental clays are actually relevant, so these oxide-based studies are in direct opposition to abundant evidence for a clay-based model. To fully quantify the percentage of studies that have used oxides over clays would require an extensive literature review. The primary use of oxides neglects one of the important characteristic of dust particles: their structure. Using oxides reverts to the idea of a homogeneous dust storm where all particles have one oxide structure. Clays, which can have a variety of structures, would be part of a heterogeneous model due to the diversity in their elemental composition and structure. The homogeneous model of mineral aerosol would assume that even with all of these different elements and dust types present, all would follow one type of reactivity and maintain the same effects throughout a storm.

Dust particle diameter and weight also dictate the relevance of different minerals in atmospheric reactions. As common sense would affirm, particles with a smaller diameter (which are usually lighter) remain suspended in the air for longer periods of time. In monitoring major dust events, the particles with longest-range transport and the greatest period of time suspended are those with diameters from 0.5-16 μm ¹⁵, and certainly less than 30 μm ⁸. Due to the effects of gravitational settling, large particles with diameters above these ranges quickly fall out of storms and clouds, leaving only the smaller particles to react and affect the chemical composition of the atmosphere. Clays, especially aluminosilicates, and quartz generally have smaller diameters than larger, pure particles (like Al_2O_3). We will show that a variety of different aluminosilicate clays and quartz have diameters within the relevant ranges listed in literature, while pure Al_2O_3 would be greatly impacted by gravitational settling due to the large measured diameters of their particles.

1.2 The Surface Structure of Mineral Dusts

Our work focuses on the relationship between the surface of a dust and the products observed. Based on the outdated homogeneous laboratory modeling of mineral aerosols, an assumption was made that the surfaces of elemental oxides were a valid representation of the total surfaces that composed actual dust storms. Even with the discovery that aluminum is only found in mixed elemental clays and the large particles do not remain in storms for long range transport, oxides were still used because it was assumed that they would act in the same way as a mixed clay. For aluminosilicates, the assumption was made that Al_2O_3 and SiO_2 together would yield the same reactivity as a mixed clay, but was this truly representative of mineral dust reactivity? For this assumption to be true, it would indicate that silicon and aluminum have no effect on one another in the surface structure of a clay and they would act in the exact same way as their oxide forms, therefore we should find the same surface sites on all oxides as we would on clays. **Figures 7-9** show quartz (SiO_2), Al_2O_3 , and kaolinite to demonstrate the structural variability between elemental oxides and clays. These structures clearly indicate different surface sites present on all of the dusts, so it is unlikely that the homogenous model and its assumptions will hold true.

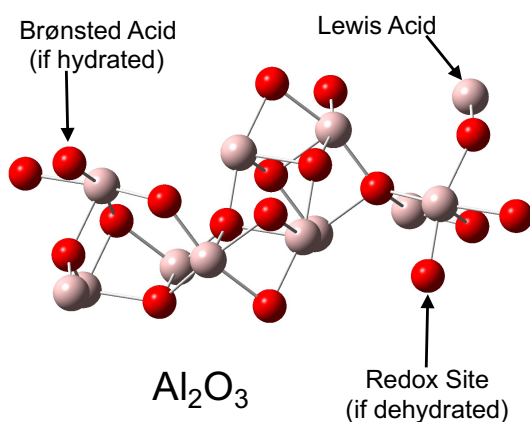


Figure 7: Gaussian Structure of Al_2O_3 with different reactive sites identified. The structure is dehydrated, so the location of redox and Brønsted sites is dependent on areas of hydration. Al is pink, O is red.

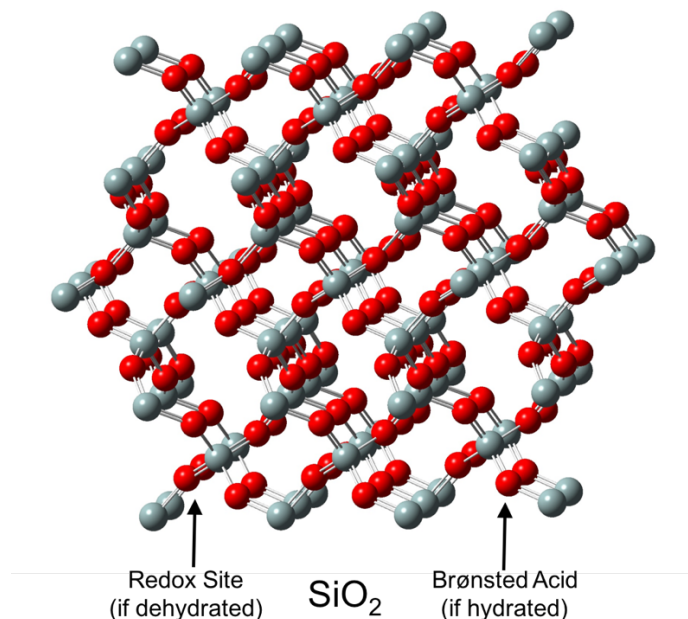


Figure 8: Gaussian structure of SiO₂ with redox and Brønsted sites identified. The structure is dehydrated, so the location of redox and Brønsted sites is dependent on areas of hydration. Si is grey, O is red.

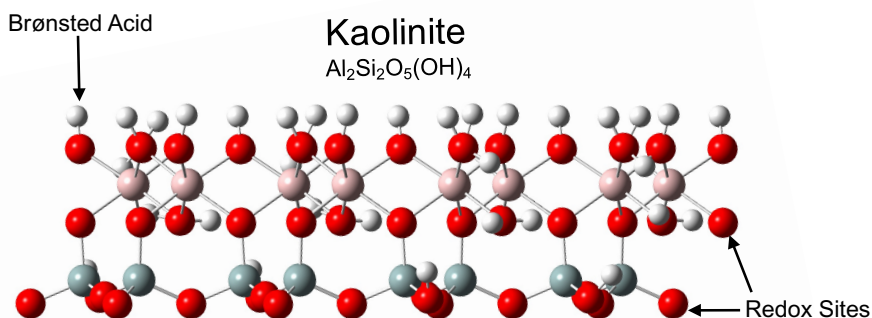
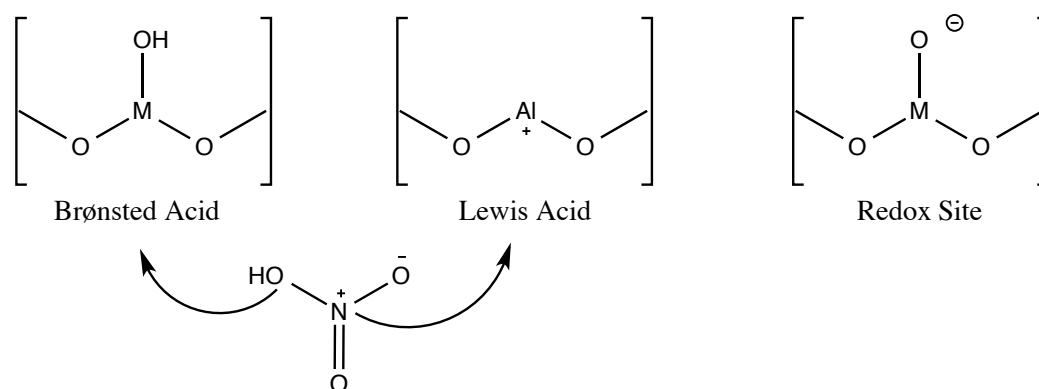


Figure 9: Gaussian structure of hydrated kaolinite with Brønsted and redox sites identified. Si is grey, Al is pink, O is red, H is white.

All of the above mineral surfaces have been shown to contain different reactive centers or oxygen sites including Lewis and Brønsted acidic sites or redox sites. For clarity, this study differentiates Lewis acids and bases and Brønsted acids and bases as in Busca et al¹⁶. Lewis acids, which accept an electron pair to form covalent bonds due to incomplete electronic groups, are seen as the more general grouping of acids because of their independence from water¹⁶. Lewis acids are usually associated with unsaturated cation centers and are therefore electron deficient, such as exposed metal ions at the mineral surface as shown on Al₂O₃ in

Figure 7. These acids are likely to accept more electrons due to their deficiency. Brønsted acids are “hydrogen-containing species able to release protons”, and are therefore a narrower group because the acids must contain an acidic hydrogen as opposed to solely needing the ability to accept electrons. Exposed hydroxyl-groups can be Brønsted acid sites because the protons on these sites can easily be released depending on the acidity of the group. An example of a Brønsted acidic site is most easily identified on kaolinite in **Figure 9**. In addition to acidic sites, all mineral aerosols have the ability to form redox sites and dust storms are associated with an increase in oxidative potential¹⁷. The redox sites are formed when edge oxygen is only bound to the mineral center and therefore has a δ^- or full negative charge on the oxygen. These redox sites are likely primarily oxidative and they add an epoxide ring across double bonds as will be shown. Clays and oxides have very different acidic properties due to the different coordination of the metal ions with their neighboring internal oxygen atoms as well as with surface or interlayer water¹⁸, so it is important to know the structure of mineral samples to describe and understand the mechanisms of reactions on the sample surfaces. **Scheme 1** displays the different types of reactive sites on dust surfaces.



Scheme 1: Different types of reactive sites on the surface of mineral aerosols. Nitric acid was shown to act as a Lewis or Brønsted acid on different mineral surfaces.

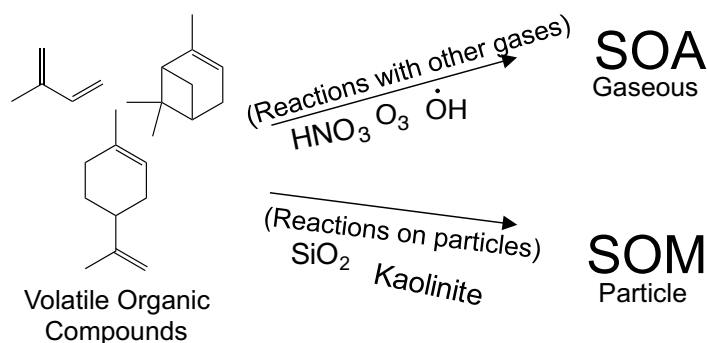
We will show that the assumption of elemental oxides acting in the same way as clays is suspect. Additionally, substituting different elements next to one another in a mixed elemental clay surface has an effect on reactivity as compared to pure aluminum oxide. We believe that $\text{Al}_2\text{O}_3 + \text{SiO}_2$ is not reactively equivalent to aluminosilicate clays, so the oxides (besides SiO_2) should not be used in laboratory models. SiO_2 is present in dust storms and therefore remains valid as a component of models of atmospheric reactions.

1.3 Reactions of Mineral Dust with Trace Atmospheric Gases

Aside from mineral aerosols, a variety of other anthropogenic and natural trace gases contribute to the profile of the atmosphere. Greenhouse gases, ozone, hydro- and halocarbons, and acids are among major volatile molecules studied in conjunction with mineral aerosols. Acids, such as nitric and sulfuric, have been shown to react readily with mineral aerosols, making these species major sinks for atmospheric acid¹⁹. Analysis of storm compositions have identified several nitrate and sulfate species attached to particles²⁰, and dust storms have been implicated in the loss of 95% of aerosolized nitric acid during events²¹. Mineral dusts have a heterogeneous impact on nitric acid abundance due to the adsorption onto the dust surface and further reactions with other adsorbed species²¹. The different reactive sites on mineral dusts, as previously described, can interact with nitric acid to produce either nitrates or just adsorbed acid. Due to the ability of mineral dusts to act as sinks for acid, we incorporated nitric acid into our experiments to account for variability in surface acidity.

Additional sources of mineral dust “aging” are reactions with volatile organic compounds (VOCs), as we modeled in this study. Our lab has proposed that a secondary organic product also forms due to reactions of VOCs occurring on a mineral dust surface, and this product would already be adsorbed to the dust particle. The new organic products formed

can be called secondary organic matter (SOM) (**Scheme 2**), and this lab has predicted and shown that and these new particulates can have a variety of effects on ice nucleation, CCN formation, and forcing²². Secondary organic products should not be a secondary thought as their name suggests as they have significant effects on the atmosphere.



Scheme 2: Formation of secondary organic aerosol (SOA) and secondary organic matter (SOM) from volatile organic compounds. Reactions with gases that form gaseous species are designated as aerosols, but when reactions occur on particles and products are adsorbed onto the surface of those particles they are classified as SOM.

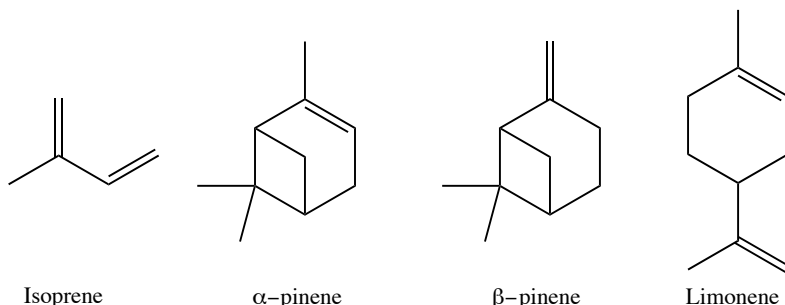


Figure 10: Isoprene and common monoterpenes. Monoterpenes are composed of two isoprene units.

While reactions of some VOCs with other atmospheric species are being studied, such as reactions with free radicals and ozone, their uptake on mineral dusts is not yet well understood. These compounds, which include a variety of halo- and hydrocarbons are composed primarily of isoprene and its derivatives, monoterpenes (**Figure 10**). Volatile organics have been shown to produce secondary organic aerosol (SOA) in reactions with other atmospheric particles (**Scheme 2**), and one study used computer models to quantify the total SOA production, which they found to be 27 Tg/yr²². This is a relatively small amount

compared to the more than 6000 Tg/yr of GHGs released, but lack of knowledge on the effects of SOA makes their study essential. The Great Smoky Mountains, a mountain range in the southeastern US, are known for their blue smoke-like haze. This haze, similar to what is seen over large cities, is known to be due primarily to volatile organic compounds, specifically terpenes²³. The vegetation in the Great Smokies is the main source for the haze, but additional gaseous pollution has contributed to decreased visibility in recent years²⁴. Trees and other vegetation in major mountain ranges and forests around the world emit large amounts of biogenic VOCs, which can then travel through the atmosphere or react with passing dust storms. In large concentrations they form the blue haze characteristic of many large forests. In addition to the biogenic sources, gaseous pollution causes large amounts of VOCs to be released. Of all VOC anthropogenic sources, fossil fuel burning, industry, chemical processing and other aerosol wastes are the major emitters of a variety of these compounds, excluding methane. The effects of light reflecting off of these compounds or causing them to react is one of the major causes for photochemical pollution²⁵. As was previously discussed, light scattering effects of gaseous species have a large variability for radiative forcing, and thus warming and cooling. Photochemical pollution in the form of increased light reflected back to earth, and therefore more heat trapped, or in the form of new gaseous pollutants (ozone) being formed through atmospheric reactions are concerning. As ozone precursors and secondary gaseous pollutant producers, VOCs and their environmental impacts need to be closely monitored²⁶. Additionally, due to the increase in emission of VOCs by plants as temperature increases²⁶, their anthropogenic emission must be closely monitored in relation to global temperature increases. Climate change due to gaseous pollution causing abnormal warming

and cooling will only act to increase the amount of biogenic reactants and could contribute to a cycle of negative environmental impacts.

VOC's are of particular interest to the government and to environmental advocates because they have been labeled by the EPA as "ozone precursors" since some reactions of these trace gases with other species such as nitrogen oxides produce ozone, especially at low altitudes²⁷. Ground-level ozone is highly toxic and causes lung and eye irritation, but stratospheric ozone is helpful because it prevents excess UV radiation from reaching earth²⁸. This reactivity makes VOCs a concern for the environment and potentially for human health. In the Clean Air Act, as amended in 2004, VOC's were addressed directly and the lack of information on their reactivity was brought up as a government concern. One of the goals of the act was to "improve the understanding of the mechanism through which anthropogenic and biogenic volatile organic compounds react to form ozone and other oxidants"²⁷. The Clean Air act also provided limits for the amount of VOCs which could be included in consumer products, especially aerosols which could increase ozone concentrations both indoors and outdoors. Secondary Organic Aerosols, or SOAs, can form as a result of VOC oxidation and subsequent condensation into particles.

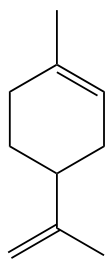


Figure 11: Structure of limonene, the VOC that was used for this research.

Limonene, a monoterpene (**Figure 11**), is one of the VOC's investigated in this lab, and it is the compound the original research by Staniec was based on. Limonene, which is

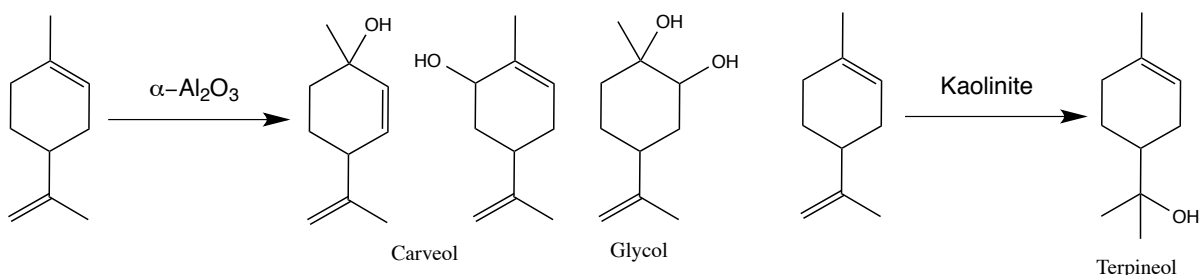
especially reactive and interesting due to two double bonds, one inside a hexane ring (endo-unsaturation) and one outside (exo-unsaturation), give multiple reactive areas within one compound. Of the annual monoterpene emissions, limonene has been modeled to compose about 20%²⁹, though its contribution is largely dependent on location³⁰. This high percentage makes limonene a very relevant compound atmospherically and demonstrates the necessity of this study in furthering our understanding of this compound's chemistry. Through studies with limonene and hydroxyl radicals, one of the more widely studied pathways for limonene reactivity in the atmosphere, limonene was determined to have a high particle yield (23-94%) compared to other terpenes, further contributing to its importance as a precursor for SOA³¹. Currently, data has shown that the lifetime of limonene in the atmosphere is likely about forty-to-eighty minutes with concentrations ranging from parts-per-trillion (ppt) to parts-per-billion (ppb)³²; due to the inability of current models and studies to accurately account for total recorded SOA production, it is important that further work is done to understand this compound's lifetime and effects.

It is important to note that this paper is describing only SOM because all of our products are adsorbed to dust particles. Current research fails to distinguish between SOA and SOM because so little work is being done on products absorbed to pre-existing atmospheric particles. Due to the size of the particles and their potential for different atmospheric properties, like CCN, they should be distinguished and studied individually. The SOA products of reactions with limonene and other volatile organics have been noted as a significant source of the haze inducing fine particles³³. The smallest of these particles are classified as PM_{2.5}, which is particulate matter with a diameter of 2.5 microns or less; these particles are heavily regulated by the EPA. The health and environmental impacts of these fine particles as a whole have been

studied extensively in recent years, and negative health effects due to inhalation of these compounds as well as decreased visibility due to haze have been noted. Not all secondary organic products fall within PM 2.5 though, because the size of these particles can increase past 2.5 microns; SOM particles generally have a larger diameter than 2.5 microns, but they still have similar harmful health effects. It is important that we understand the effects of reactions with VOCs as they may contribute to significant pollution and reduction of visibility. Research with this class of trace gases has been conducted as computer modeling studies, gas phase reactions, and heterogeneous reactions, but due to the variety of reaction types possible, it is difficult to account completely for the measured SOA production with one model³⁴. This thesis attempts to provide a better description of SOM as opposed to SOA and use our reactions to account for some of the missing SOA in current models. If researchers fail to recognize SOM, they will be leaving out a significant number of products from reactions with volatile organics, so this thesis can act as a new model for further research.

1.4 Goals of the Current Study

This lab had previously studied the effects of acid on the reactive uptake of VOCs on both oxide and clay surfaces. Unexpectedly, the oxides and clays tested produced very different product mixtures, though the expectation was for a similar reaction on the different surfaces due to the elemental relevance of both aluminum oxide and aluminosilicate clay³⁵. Allison Staniec found that Al_2O_3 produced a mixture of products including limonene glycol and carveol, while kaolinite formed only one product, terpineol³⁵ (**Scheme 3**). In an attempt to understand the differences between the surface sites that would cause such different reactivity, this study expands upon the previous research to quantitatively and qualitatively compare a



Scheme 3: Products formed in the reactions by Staniec on Alumina and Kaolinite dust. Alumina produced a product mixture of carveol and limonene-glycol, but kaolinite had a single product: terpineol.

variety of clay and oxide surfaces in addition to an atmospheric dust sample. We systematically studied a variety of different dusts including both elemental oxides and mixed aluminosilicate clays to assess whether or not the current model of oxide reactivity being representative of clays was false. This assessment was done by comparing product formation and proposed mechanisms for each product, reactive uptake of limonene on the surface using kinetic data, and particle size changes.

Using Diffuse Reflectance Infrared Fourier Transform Spectroscopy (DRIFTS) and Gas Chromatography with Mass Spectrometry (GC-MS) we monitored reactions of limonene on a variety of mineral dusts and quantified and identified products of these reactions with the goal of identifying differences between different dust surfaces. Brunauer-Emmet-Teller (BET) theory surface area analysis, Attenuated Total Reflectance Fourier Transform Infrared (ATR-FTIR) Spectroscopy, and a light-scattering particle sizer were used to supplement the measurements on the dusts and calculate reactive uptake of limonene on each surface. Additionally, reactions with a nitric acid pre-treatment were used to model the atmospheric sinks for nitric acid on mineral dusts. Labelling experiments were used for confirmation of mechanistic hypothesis and further understanding of surface chemistry in relation to adsorbed water.

The experimental methods of this project are detailed in Chapter 2, including the sample and reaction preparation, spectroscopy, and analytical techniques used. Chapter 3 discusses the observed products of each reaction and propose mechanisms for the formation of each based off of labelling experiments and similar reactions reported in literature. Additionally, this chapter discusses the relationship between mechanisms observed and the structure of different mineral surfaces. Chapter 4 explains the calculated reactive uptake of limonene on each dust sample and attempts to justify altered reactivity due to nitric acid coating. This chapter is primarily a discussion of the kinetics observed in each reaction and thus the relevance of each mineral aerosol in actual atmospheric reactions. Chapter 5 summarizes of all observed data and conclusion of this thesis. I will propose future work to improve understanding of VOC uptake on mineral surfaces as well as propose a different model for improving future research.

Chapter 2: Material and Methods

Reactions of limonene gas with mineral dust samples were performed in a Diffuse Reflectance Infrared Fourier Transform Spectroscopy (DRIFTS) chamber with a continuous flow of humidified air. The DRIFTS chamber allowed infrared monitoring of the dust surface to visualize the adsorption of organic products to the surface (**Figure 12**). The first section, gas preparation, will describe the methods for achieving constant flow of humidified air and

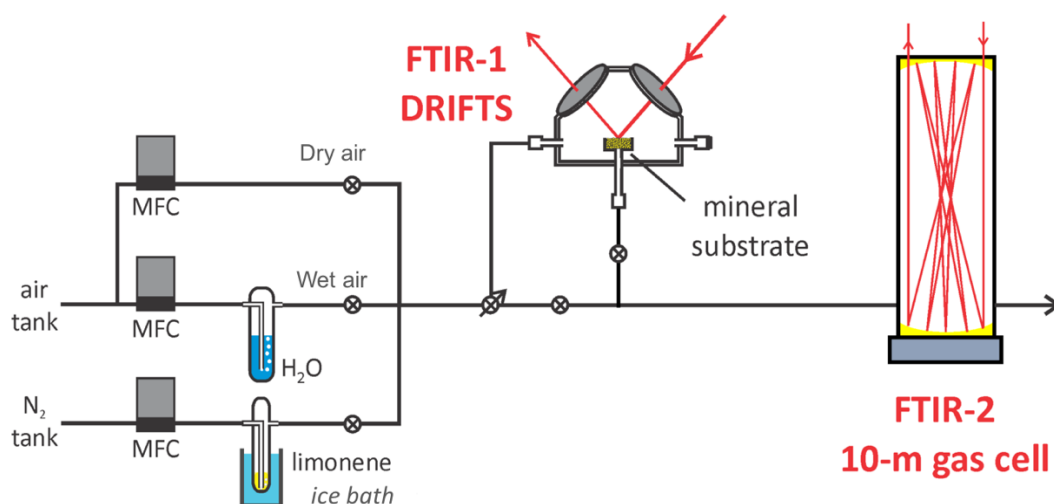


Figure 12: Reaction preparation and monitoring setup. Limonene and humidified air were mixed prior to exposure to mineral dust in the DRIFTS FTIR. Gas flowed through the substrate into an exhaust and spectra were recorded of the gas content in the 10 m Gas Cell FTIR prior to exit from the system.

gaseous limonene. Reactions were also performed with isotopic labelling of products by ¹⁸O_{H₂ to provide markers indicative of the mechanism. Nitric acid pre-treatments of the dusts were used as a model for atmospheric sinks of acid on mineral surfaces. The second section describes the infrared technology used to monitor the reactions and air flow. Preparation and handling of the mineral dust samples will be described in the third section. Product extraction off of the dust surface was performed to identify and quantify adsorbed species on each sample. The fourth section will describe extraction methods used and the quantification using gas chromatography and mass spectrometry in combination with a fifth section on surface area}

monitoring with BET analysis. Finally, the method of calculating reactive uptake coefficients, which relies on all previous methods for different variable values, will be described as they were the final figures calculated to understand dust kinetics.

2.1 Gas preparation

Air at 30% relative humidity (RH) was mixed using mass flow controllers (MFCs)³⁶. Dry air (about 220-230 sccm) entered the system from a compressed air tank. Wet air (~95-100 sccm) entered the flow by splitting the carrier gas at a T-junction (**Figure 12**) and controlling the air flow into a water bubbler maintained at 25°C. Compressed nitrogen gas (~30 sccm) was used as the limonene carrier. N₂ flowed through a bubbler of liquid (R)-(+)-limonene (Sigma-Aldrich, 97% stated purity, CAS# 6-22-12) cooled to 0°C in an ice bath to lower the vapor pressure of the limonene. Limonene at a lower vapor pressure could be exposed to an increased flow rate of 30 sccm, as opposed to the original 3 sccm, without altering the concentration. The increased flow rate maintained the limonene concentration between 34 and 61 ppm (excluding one experiment with Arizona Test Dust and no nitric acid) for each experiment and kept constant at the start of the reaction so as to maintain a constant limonene concentration in the DRIFTS reaction chamber. A similar concentration of limonene was necessary for comparison of the various mineral dusts. Additionally, to improve flow rate control, tubing was dried between experiments by using a high airflow, 150 to 200 sccm.

2.1.1 Isotopic Control Experiment

A control reaction with nitrogen gas, instead of air carrier gas, and isotopically labeled water was run to determine the mechanism of reaction. This isotope labelling experiment was performed only once on Arizona Test Dust. H₂O¹⁸ (Sigma-Aldrich, CAS#14314-42-2, 99%

stated purity) replaced deionized water to maintain 30% relative humidity. Compressed N_{2(g)} was used as the limonene carrier.

2.2 Reaction Monitoring

To initiate the reactions, limonene flow was directed into the reaction chamber and spectra were recorded using Diffuse Reflectance Infrared Fourier Transform Spectroscopy (DRIFTS) on a Thermo Nicolet 6700 FTIR with an MCT-A detector. 256 scans were averaged to create the spectrum at each time point. Initial background scans were recorded on OMNIC software prior to limonene exposure, and once the reaction began, a series of spectra were recorded until the reaction was complete. Reaction completion was determined by the slowing of product growth monitored using the C-H stretches between 2796 cm⁻¹ and 3010 cm⁻¹.

To identify what dust depths were represented in the spectra, layering tests with Arizona Test Dust and kaolinite were conducted. Varying depths of Arizona Test Dust covered the kaolinite at the bottom of the cup while spectra of the surface were collected (**Figure 13**). The characteristic peak of kaolinite between 3630 cm⁻¹ and 3610 cm⁻¹ was integrated and compared with the depth in **Figure 13**, demonstrating that the DRIFTS spectra were only representative of the very surface of the sample. This information influenced the sample splitting procedure as discussed in section 2.4.

Limonene concentration in the gas phase was monitored using a second Thermo Nicolet 6700 FTIR (Thermo Scientific), with a 10 m pathlength. Carrier gas and limonene bypassing the DRIFTS chamber prior to the start of the reaction was monitored on OMNIC software by comparison to flow of only humidified carrier gas. Once limonene concentration remained stable and had an integration of 2.5 to 3 under the peak in Figure 3, the dust was

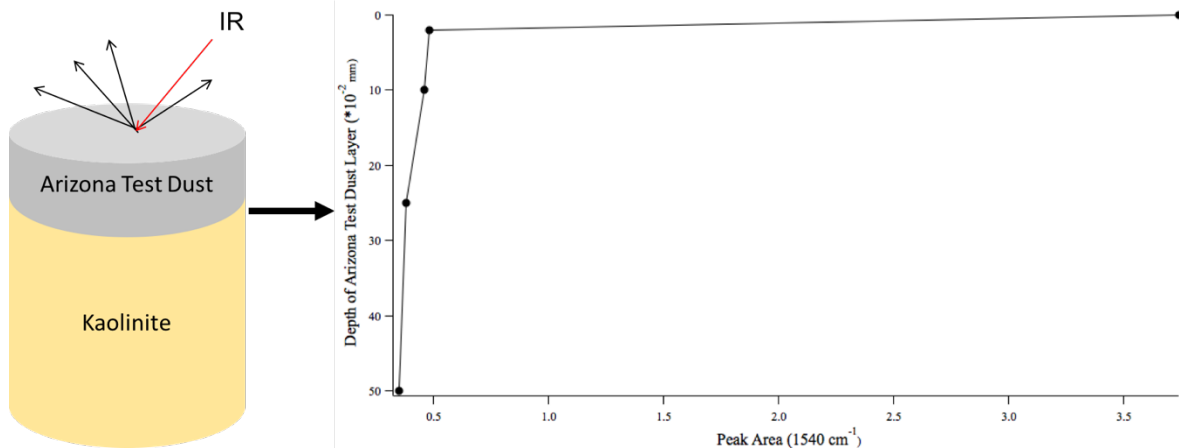


Figure 13: Layering experiments with different amount of kaolinite confirmed that the IR only scanned the very surface of the dust. A figure of the layering method with Arizona Test Dust over kaolinite, and integration of kaolinite's characteristic peak between 3630 cm^{-1} and 3610 cm^{-1} .

exposed to the continuous limonene flow and monitoring began. Gas-phase spectra were recorded of the reaction exhaust, which contained the limonene concentration.

Kinetic data were collected for each experiment by integrating the area under the product characteristic peak at 2796 cm^{-1} to 3010 cm^{-1} using IgorPro software. Humidified dust backgrounds were subtracted prior to integration. Integration was plotted against time and the final integration was used to convert the data to surface concentration against time. Surface concentration was calculated using the sum of products identified on the GS-MS, as discussed in section 2.3, and the surface area found using the BET, as discussed in section 2.5.

2.3 Dust Preparation

The dust surfaces used had variable composition and structure. The Arizona Test Dust (Powder Technology Inc, ISO 12103-1 A2 Fine) sample and others⁴ have high fractions of aluminum and silicon in the elemental composition studies, so clays and oxide aluminosilicates were chosen. The pure oxides used were SiO_2 (Aldrich Chemical Company Ltd, 99.6% stated purity, CAS# 60676-86-0), additionally known as quartz; $\gamma\text{-Al}_2\text{O}_3$ (Alfa Aesar, 99.997% stated purity, CAS# 1344-28-1, Stock#42576); and $\alpha\text{-Al}_2\text{O}_3$ (Alfa Aesar, 99.997% stated purity,

CAS# 1344-28-1, Stock#35839). These oxides were chosen based on their frequent use in laboratory models. The clays studied were Ca-rich Montmorillinite (Source Clays Repository, STx-1b), Illite (Source Clays Repository, IMt-1) and Kaolinite, $\text{Al}_2\text{Si}_2\text{O}_5(\text{OH})_4$ (Fluka Analytical, CAS#1318-74-7). Pyrophyllite was initially considered, but was excluded due to the impurities present in the dust produced by flaking from a crystal and ball-milling. CaCO_3 (Sigma-Aldrich, 99.995+% stated purity, CAS# 471-34-1) was used to test the reactivity of the setup with carbonates. Arizona Test Dust was dried at 100°C initially due to the wet texture of the dust, but there was no additional temperature exposure to the dusts to eliminate the possibility of altering the surfaces. Due to the increased pressure on the dust during reactions, calcite (CaCO_3) was used in some experiments to maintain a flat surface in the sample cup (**Figure 14**). The bottom layer of CaCO_3 was about 0.5mm deep and it acted as a barrier to stop the sample dust from forming a hole and entering the exhaust tubing. As shown in **Figure 13**, only the surface of the dust sample was being scanned by IR, so the deep layer of CaCO_3 would not affect the kinetic data. CaCO_3 was also found to not be reactive in these conditions, so it did not interfere with product identification. Additionally, a small aluminum screen was placed at the bottom of the sample cup in every experiment to protect the tubing and act as a base on which the dust could be packed.

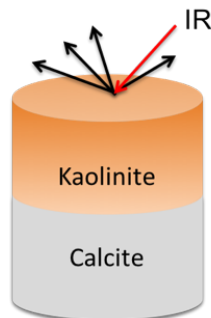


Figure 14: Layering method for dusts samples with unreactive calcite. Calcite was used to prevent air pressure from forming a hole in the sample. Only the top layer was extracted for GC-MS, and the IR beam only analyzed the surface of the dust sample, so calcite did not interfere with the data.

To model the dust surfaces as sinks for atmospheric acids, a HNO₃ vapor, generated over a mixture of concentrated liquid HNO₃ (15M) and H₂SO₄ (18M), was collected in a stainless steel lecture bottle (~8-15 Torr), then pressurized to 350-370 psi with Helium. The mixture ensured that HNO₃ would be protonated because water would first react with the concentrated H₂SO₄. The pressurized canister was connected to the DRIFTS chamber through an additional input and allowed to empty by flowing through the dust and out of the exhaust. The dust prior to HNO₃ exposure was dried for 30 minutes using air flow at 0% RH to eliminate any reaction of HNO₃ with surface water and prevent water from occupying surface sites. Following HNO₃ coating, the dust surface was exposed to humidified air until the relative humidity was stabilized at 30%.

2.4 Product Identification

After the reaction concluded, each dust sample was separated into three layers, massed, and then the adsorbed organics were extracted into acetonitrile. The very top dusting was used for product quantification because it corresponded to the surface concentration of product monitored by the DRIFTS (see **Figure 13**). The middle and bottom layers split the remaining dust. Extraction was performed by adding massed acetonitrile (CH₃CN) (Pharmaco-Aaper, CAS# 75-05-8), sonicating for 20 minutes, and filtering to remove all dust from the products. Whatman 2µm filters were used due to sample contamination by high molecular weight compounds in older 2µm filters.

Using Gas Chromatography-Mass Spectrometry (GC-MS) on an Agilent 7890A-7975C instrument, products were identified. Initial comparison to the National Institute for Standards and Technology (NIST) library databases was useful for identifying products based

on fragmentation patterns. Standards of different products were tested to confirm the identification and create concentration curves for quantification (**Figure 15**). Based on the similar slopes between all of the standards, it was determined that the products had similar response ratios and a slope average was used to quantify products without standards or unknowns. Limonene-diol (Sigma Aldrich, 97%, CAS#38630-75-0), (R)-carvone (Sigma Aldrich, 98%, CAS# 6485-40-1), (-)-carveol (Sigma Aldrich, 97%, CAS# 99-48-9), and α -terpineol (Sigma Aldrich, CAS# 10482-56-1) were used as standards without further purification. Only products eluting in the first 32 minutes were considered to exclude the filter contamination at higher molecular weights and later elution times.

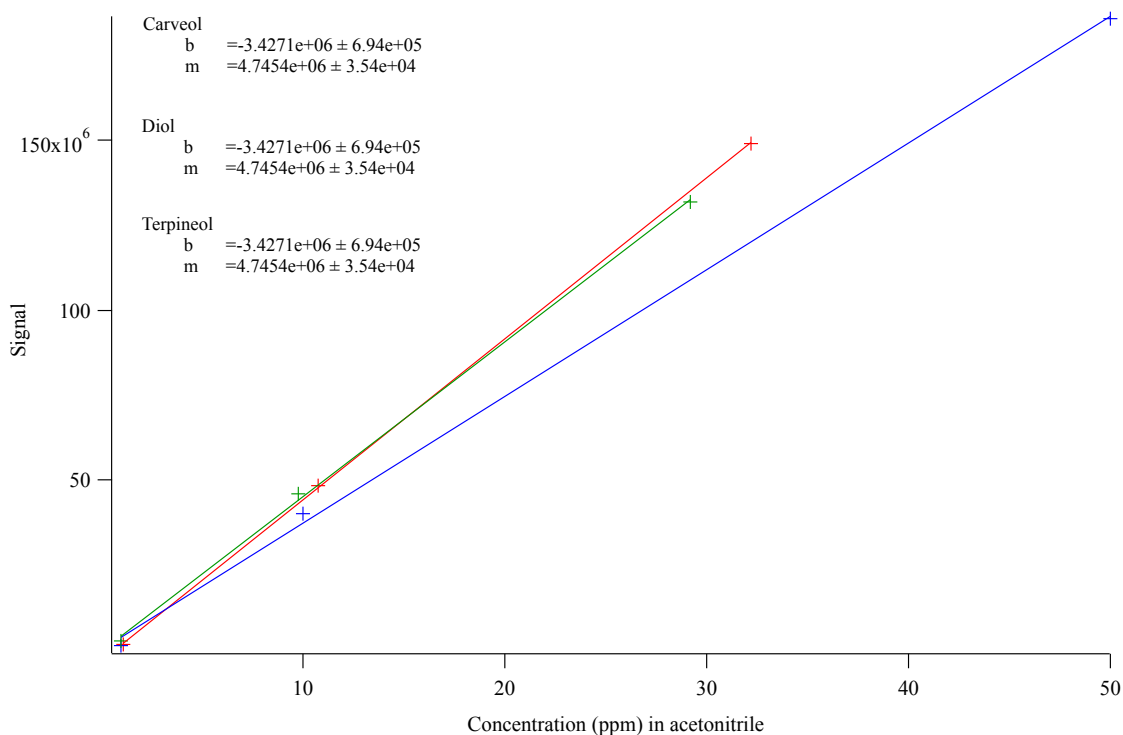


Figure 15: Concentration curves for carveol, limonene-glycol (diol), and terpineol in acetonitrile.

To clarify the product IR spectra, samples were dried onto a diamond crystal after extraction in acetonitrile by N_2 carrier gas. The crystal on a Smart ITR Diamond attachment for a Nicolet iS10 FTIR (Thermo Scientific) recorded product spectra without the coupling to

the surface of the dusts that slightly distorts DRIFTS spectra. Using this clarification, some peaks were identified as effects of the dust surface and not corresponding to the products.

2.5 Surface Area and Particle Size Profiling

The surface area of each dust type was calculated using a Nova2000e Surface Area & Pore Size Analyzer (Quantochrome) with 9mm bulbless cells. This instrument uses Brunauer, Emmet and Teller (BET) theory of gas adsorption onto solid particles to calculate particle surface area and pore size. The samples were degassed at 200°C for 12+ hours prior to N₂ adsorption while the sample cells were cooled in liquid N₂. The instrument recorded P/P₀ and the adsorbed volume, and using Equation 1, the BET data points were calculated in Microsoft Excel. Using a 10-point calculation within the P/P₀ range between 0 and 0.4, the slope and intercept of the BET data were calculated using IgorPro software. Equation 2 was used to calculate the surface area from the linear fit. **Table 1** gives the surface area per gram of dust for each sample.

$$BET\ value = \frac{1}{V_A \left(\frac{1}{P/P_0} - 1 \right)}$$

Equation 1

$$SA = \frac{\left(\frac{1}{m + b} \right) \times \text{mass}_{\text{sample}} \times P}{R \times T} \times N_A$$

Equation 2

Table 1: BET Surface Area measurements for each dust sample with and without HNO₃ coating.

	α Al ₂ O ₃		γ Al ₂ O ₃		SiO ₂		Kaolinite		Montmorillinite		Arizona Test Dust		Illite
	No	Yes	No	Yes	No	Yes	No	Yes	No	Yes	No	Yes	No
Surface Area (m ² /g)	10.227	6.772	57.537	57.126	4.316	1.640	10.598	2.860	76.928	43.031	12.632	9.273	12.270

To test the effects of nitric acid on the surface area and gain more accurate calculations for the product concentration on samples exposed to HNO₃, samples were pre-treated with gaseous HNO₃. Using a vacuum manifold, a mixture of HNO₃ and H₂SO₄ was exposed to the

dust samples at $P \approx 0$ torr for 30-45 minutes. To confirm coating on the samples, DRIFTS spectra were recorded in a sample cup and compared to uncoated dust. The same BET calculation procedure was used with the HNO_3 treated dust.

Particle diameters were determined using a Tornado Dry Powder System on a Beckman Coulter LS 13 320 Laser Diffraction Particle Size Analyzer. The same approximate volume was used for each sample to normalize the number of particles being analyzed.

2.6 Reactive Uptake Calculation

The reactive uptake coefficient for each experiment was calculated by combining the various pieces of data into Equations 3 and 4³⁷. In Equation 3, $d[\text{diol}]/dt$ corresponds to the reaction collision rate, while Z is the total collision frequency. Reactive uptake coefficients are a measure of how many total collisions actually result in a reaction. Equation 4 is based off of the kinetic theory of gases. These calculations yielded information on the kinetics of each experiment and the aging of atmospheric dust.

$$\gamma = \frac{\text{reactive_collisions}}{\text{total_collisions}} = \frac{d[\text{diol}]/dt}{Z}$$

Equation 3

$$Z = \frac{[\text{limonene}]}{4} \sqrt{\frac{8RT}{\pi M_{\text{diol}}}}$$

Equation 4

Chapter 3: Products and Mechanisms of Product Formation of the Reaction of Limonene on Mineral Dusts

Mineral dusts were exposed to ~15 ppm limonene gas at a relative humidity of approximately 30%. Reaction spectra indicated the growth of adsorbed organics on the mineral dust surface as the reaction progressed primarily by the large C-H peak at about 2900 cm^{-1} (**Figure 16**). The dust samples were extracted into acetonitrile to identify and quantify the organic products by gas chromatography and mass spectrometry. A gas chromatogram example of the products observed on Arizona Test Dust is presented in **Figure 17a** with only the first 32 minutes of sampling displayed. No relevant or identifiable products were observed after 32 minutes. Gas chromatograms of standards of 10 ppm limonene-glycol, 14 ppm carvone, and a 10 ppm carveol-terpineol mix, all dissolved in acetonitrile, are shown in **Figure 17b**. The sample showed peaks corresponding to carveol at about 16 minutes, carvone at about 18 minutes, and limonene-glycol at about 28 minutes.

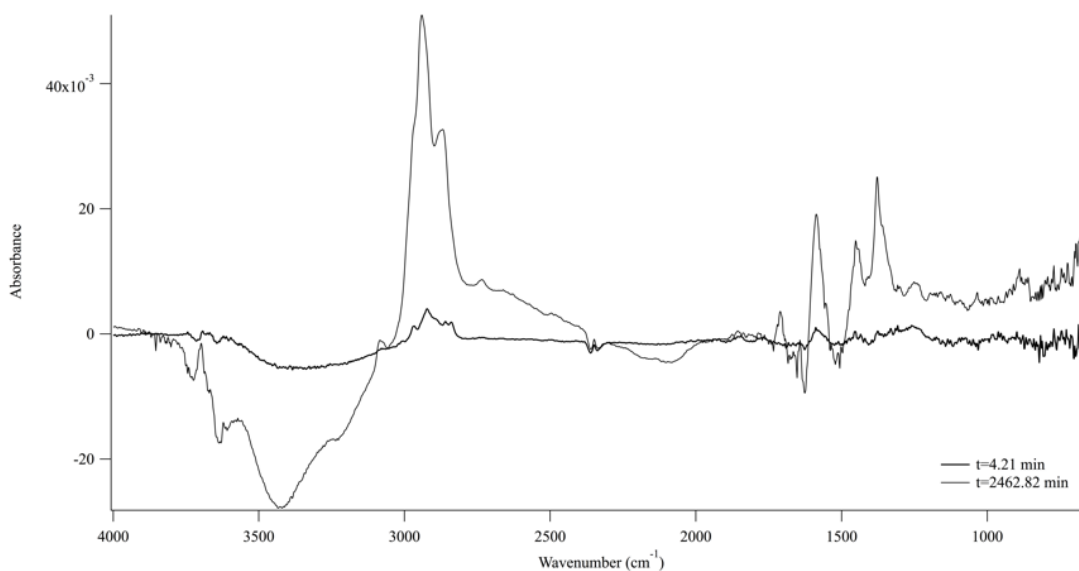


Figure 16: The final IR spectrum and the first IR spectrum of a reaction on Arizona Test Dust. Growth of an absorbance at $\sim 2900\text{ cm}^{-1}$ shows the organic product has formed on the dust surface.

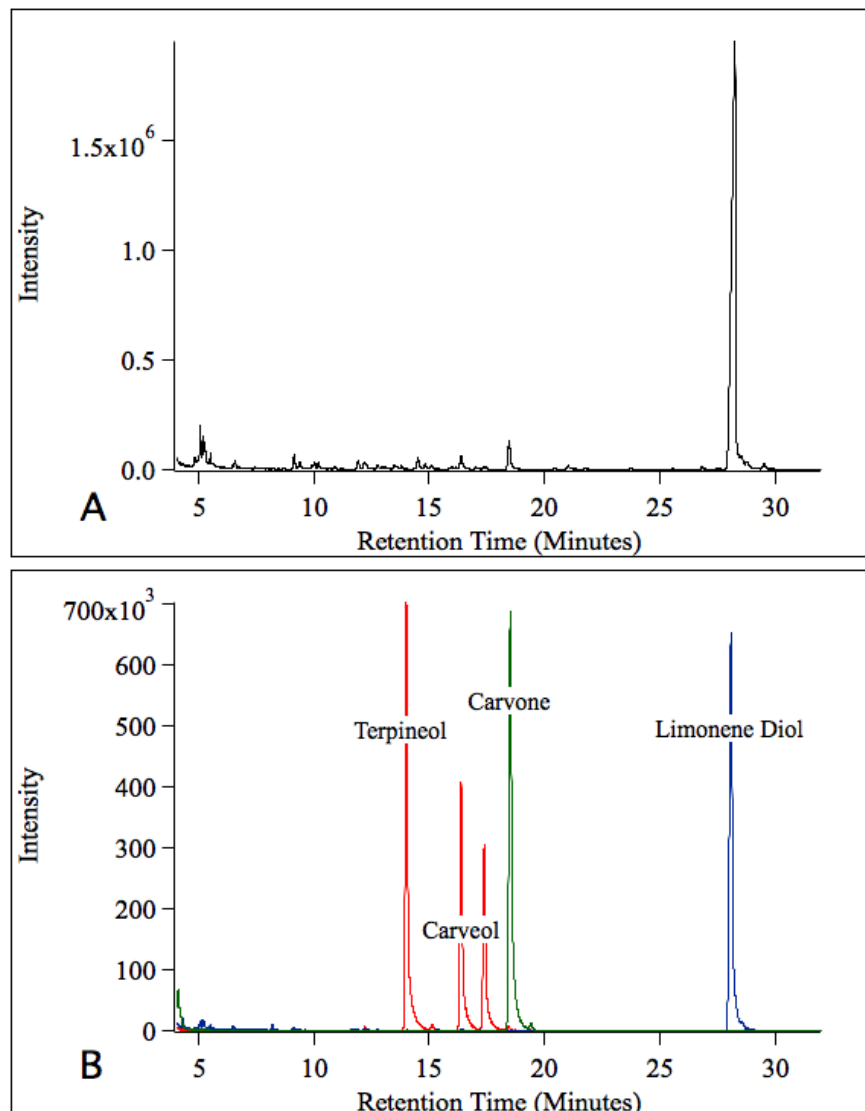


Figure 17: Total Ion Chromatograms (TICs) of products (A) and product standards (B) showing retention times and ion intensity. In graph B, standards of terpeneol, two carveol isomers, carvone, and limonene glycol (diol) were used.

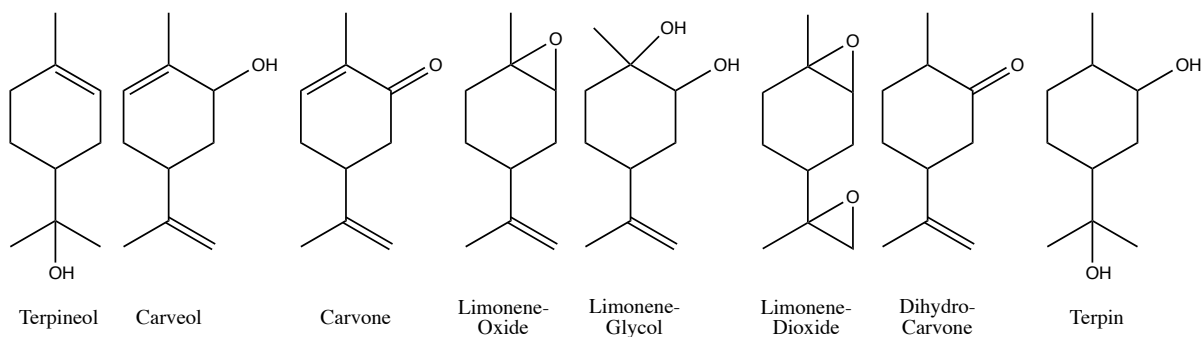
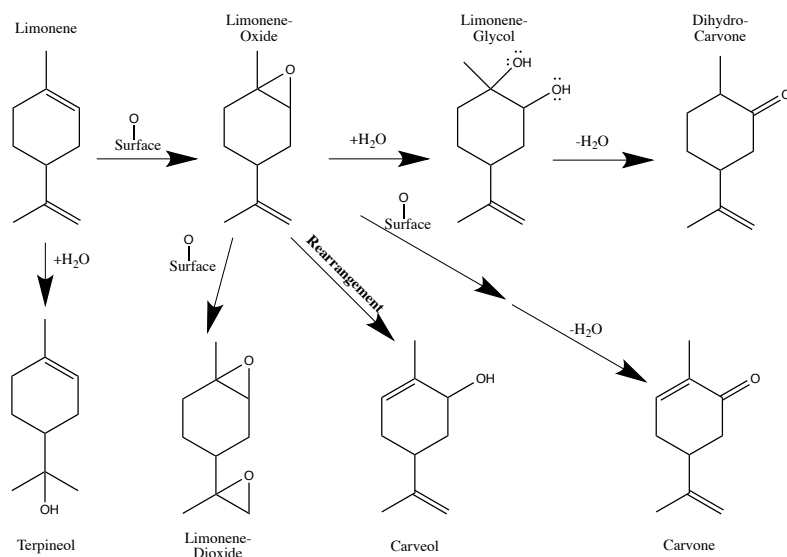


Figure 18: Structures of all identified products from reactions of limonene on mineral dust surfaces. Organized by retention time.

Table 2: Amount of each product formed during reactions of limonene on mineral dusts. Product percentages, sum in ppm, and the total amount formed (molecules/m²). Limonene glycol is consistently a major product. Compounds are listed by retention time. The top value gives the concentration of that product in ppm, while the bottom value gives the percentage composition.

	Terpineol	Carveol	Carvone	Limonene- Oxide	Limonene- Glycol	Limonene- Dioxide	Dihydro- Carvone	Terpin	Unknown	Sum (ppm)	molecules/ m ²
α Al ₂ O ₃	0.37 4.60%	2.55 31.77%	0.38 4.77%	0.61 7.59%	3.61 44.95%	X	X	X	0.51 6.31%	7.52	8.30E+17
γ Al ₂ O ₃	0.51 2.83%	9.50 53.25%	1.31 7.32%	1.20 6.74%	3.05 17.07%	X	X	X	2.28 12.80%	15.56	8.76E+17
SiO ₂	X	X	0.26 2.51%	X	10.01 97.49%	X	X	X	X	10.27	3.55E+18
Kaolinite	X	X	0.16 0.40%	X	38.89 99.60%	X	X	X	X	39.05	8.41E+18
Montmorillinite	14.34 13.32%	20.72 19.25%	5.56 5.16%	X	58.91 54.74%	1.52 1.41%	3.43 3.19%	X	3.15 2.92%	107.63	1.37E+18
Illite	X	1.24 2.68%	1.83 3.96%	X	42.93 92.70%	X	0.31 0.67%	X	46.31	46.31	6.31E+18
Arizona Test Dust	X	0.97 2.77%	0.99 2.81%	0.25 0.72%	32.03 91.43%	X	0.32 0.91%	X	0.47 1.35%	35.04	6.16E+17
α Al ₂ O ₃ + HNO ₃	X	3.46 6.41%	0.77 1.43%	0.89 1.65%	44.48 82.41%	0.71 1.32%	1.49 2.76%	X	2.18 4.03%	53.97	7.33E+18
γ Al ₂ O ₃ + HNO ₃	X	4.91 5.52%	1.13 1.27%	0.75 0.84%	73.24 82.42%	4.45 5.01%	3.35 3.77%	X	1.04 1.17%	88.86	4.45E+18
SiO ₂ + HNO ₃	4.08 16.50%	1.16 4.70%	0.87 3.54%	X	17.33 70.17%	0.54 2.20%	X	X	0.71 2.89%	20.62	1.55E+19
Kaolinite + HNO ₃	X	X	X	X	19.37 100.00%	X	X	X	X	19.37	4.65E+18
Montmorillinite + HNO ₃	23.07 5.90%	X	1.74 0.45%	X	5.95 1.52%	X	X	356.71 91.18%	3.73 0.95%	368.13	1.82E+19
Arizona Test Dust + HNO ₃	X	1.01 3.73%	0.71 2.63%	X	24.68 91.00%	0.20 0.75%	0.51 1.89%	X	X	27.13	3.41E+18

All of the products identified are displayed in **Figure 18**. Quantification and product identification by GC-MS yielded the data in **Table 2**. The product distribution of each reaction was normalized based on total products to determine the percentage of each product formed. Limonene-glycol was present in all reactions and was a major product. Product formation is limited by the exposure of limonene to surface sites, so once the sites become saturated with product, there is limited possibility for reactivity. There was a consistent increase in total product formed when the reactions were performed with dust pre-exposed to HNO₃, so the exposure may have acted to allow further sites to be available, or different sites. Additionally, there was consistently more product formed on clay surfaces -kaolinite, montmorillonite, and illite- in comparison to aluminum-oxide surfaces. This structural difference alone is an indication that metal oxides differ greatly from mixed elemental clays. Reactions with the pre-exposure to nitric acid maintained the pattern of increased product amounts formed on clay surfaces. This chapter will discuss possible mechanisms for each product observed, as summarized in **Scheme 4**, and their relation to the mineral dust structure.

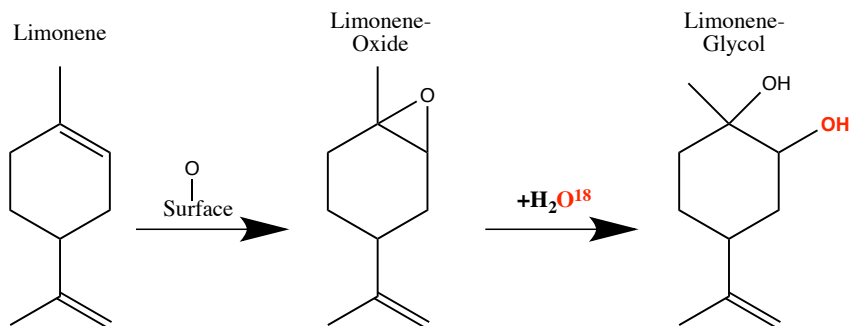


Scheme 4: Proposed mechanisms of product formation for all products observed from reactions of limonene on mineral dust samples. Limonene-glycol was a dominant product in all reactions and carvone was observed in most reactions.

3.1 Mechanistic Descriptions of Each Observed Product

3.1.1 Limonene Glycol as the Dominant Product

A proposed mechanism for the formation of limonene glycol, and its intermediates will be discussed. In Table 1 it can be observed that limonene glycol is the major product in all reactions excluding α -Al₂O₃ and γ -Al₂O₃. We hypothesize that the glycol formed through an epoxide intermediate and subsequent breaking of the epoxide to yield a double substitution of alcohol groups at the original site of endo-unsaturation. As seen in **Scheme 5**, the epoxide would form as a result of reaction with surface reactive oxygen. Removal of an oxygen from a M-O bond, where M could be either Al or Si, would form a reduced surface site on the dust. Where oxygen oxidizes the colliding limonene, or other molecule, the surface is reduced and forms a cation. This reduced site would return to its original state due to re-oxidation from adsorbed molecular oxygen gas³⁸. Additionally, after removal of oxygen from the surface of the dust, there would be an exposed metal cation prior to O_{2(g)} replacement, and hydroxyl groups, or water, could adsorb to these sites and act as Brønsted bases³⁸ if the sites were not already blocked by an adsorbed product. Surface adsorbed water also acts as a reactant to break the epoxide ring formed on limonene, and generate a di-substituted hydroxyl product. Literature shows that epoxide formation in isoprene, the parent compound of monoterpenes, has been observed in the gas phase. Gas and aerosol phase experiments have shown an epoxide intermediate formed by hydroxide radicals in the gas phase, and deposition into the aerosol phase following substitution of both double bonds³⁹.



Scheme 5: Proposed mechanism for the formation of limonene glycol by way of an epoxide intermediate. Based on fragmentation patterns, one isotopically labeled and one unlabeled hydroxyl were identified after reaction of Arizona Test Dust with limonene, N₂ carrier gas, and H₂O¹⁸ at about 30% humidity.

In support of our proposed mechanism for glycol formation, isotopically labeled water, ¹⁸OH₂, showed addition of one labeled oxygen only (**Figure 19**). Air was eliminated from the reaction by using N₂ as the carrier gas, therefore the surface could not regenerate reactive oxygen from adsorbed gaseous O₂. We did see significant product formation under the modified conditions, though, indicating that regenerated oxygen sites were not necessary for product formation. This result further confirmed water breaking the epoxide as shown in **Scheme 5**, because the surface-bound oxygen was not necessary for the second step of the reaction to occur. We could not confirm the location of the isotopic addition, though we hypothesize that it likely occurs on the carbon alpha to the methyl group. Use of the O¹⁸ water provided a method for following the path of water in the reaction. If water did not participate in the reaction, then we would have expected the M-18 peak in the mass spectrum (total mass with H₂O subtracted) to remain at the same mass, 152 amu. In the MS, ionized limonene glycol is unstable, and it is therefore fragmented very easily and often loses water, thus the major peak occurs at Mass-18. Due to the uncertainty about which carbon the O¹⁸ water might add to, there was also a possibility that we would see no shift due to loss of H₂O¹⁸. The observed shift was to a mass of 154 (**Figure 19**), two units greater than the observed Mass-18 peak in

the standard. Additionally, many of the major fragments from the reaction under normal conditions had a corresponding peak with a mass 2 amu greater in the isotope reaction.

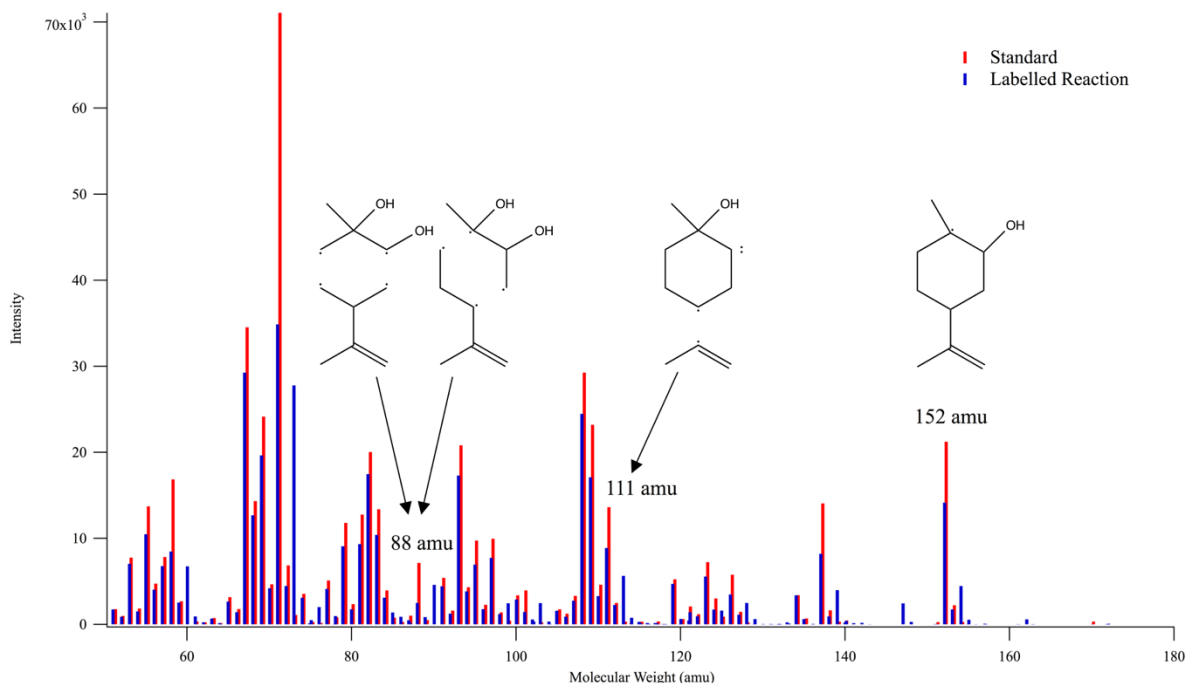


Figure 19: Overlay of raw mass spectra for limonene glycol from H_2O^{18} labelling experiment and from a glycol standard. All highlighted fragments correspond to the glycol standard and have a correlated shift in the labelled reaction of +2. The 88 amu fragment corresponds to both hydroxyls remaining together on one adduct. We can see in this figure that the mass only shifts up by two, so only one hydroxyl has an O^{18} label. The Mass-18 peak also shows a shift on +2 to 154 amu, indicating that the fragment has one O^{18} hydroxyl.

If surface adsorbed H_2O^{18} was the source of both added hydroxyl groups in the product, then the mass should have increased by 4 amu at an increase of 2 amu per additional oxygen. But, due to loss of one water from the product, we would only observe this shift if both hydroxyls were intact in the fragment, so the Mass-18 peak would not show the double addition. Notably, the fragmentation possibilities corresponding to a mass of 88 amu in **Figure 19** must contain both of the hydroxyls. The other fragments are cleaved between to two adducts, thus it is difficult to identify whether both of the added oxygen were labeled prior to splitting into different fragments. Confirmation that the fragment corresponding to 88 amu

matched when offset by +2 provided significant evidence for the single addition of water and its role in cleavage of the epoxide ring.

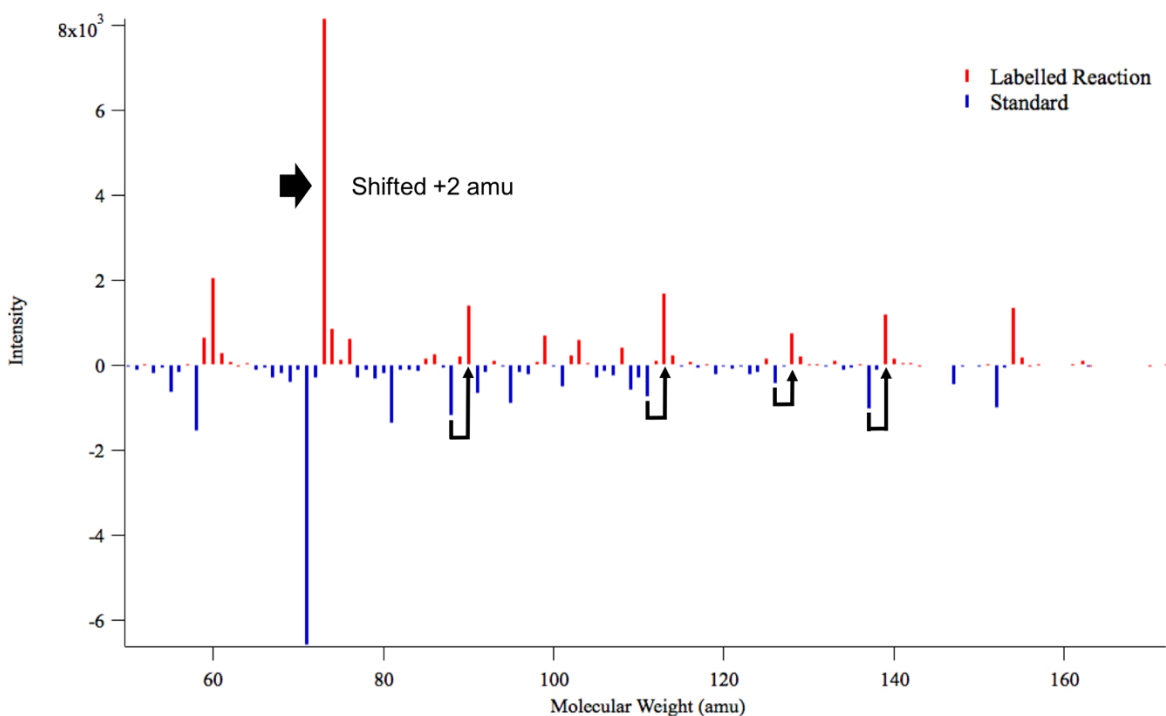
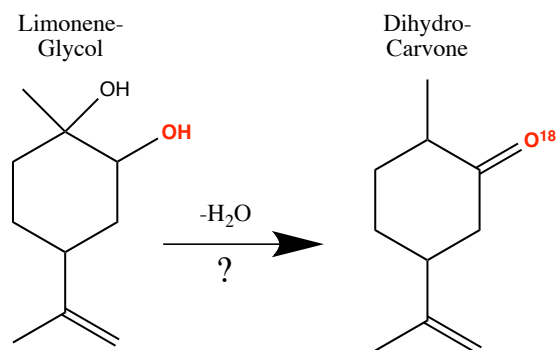


Figure 20: The difference mass spectra peaks between limonene-glycol standard (blue) and the O^{18} label limonene-glycol (red). The difference between the labeled mass spectrum and the standard mass spectrum, where peaks present only in the standard are negative and displayed in blue. The major labeled peaks are clearly shifted upwards by two units, indicating a single addition of O^{18} hydroxyl.

Finally, to visually confirm that the offset between most major fragments in the two samples was 2 amu, we found the difference between the two mass spectra for the isotopically labeled limonene glycol and the standard limonene glycol (**Figure 20**). The negative data shows peaks that were present in the standard but not in the O^{18} experiment. The positive peaks, which are clearly shifted forward by +2 amu were present in the O^{18} experiment but not in the standard. All of the fragments that contain at least one hydroxyl and are present in one of the spectra but not the other are shown in **Figure 20**, and the offset of 2 confirms only one addition of an O^{18} hydroxyl.

3.1.2 Dihydrocarvone as a secondary product after glycol formation

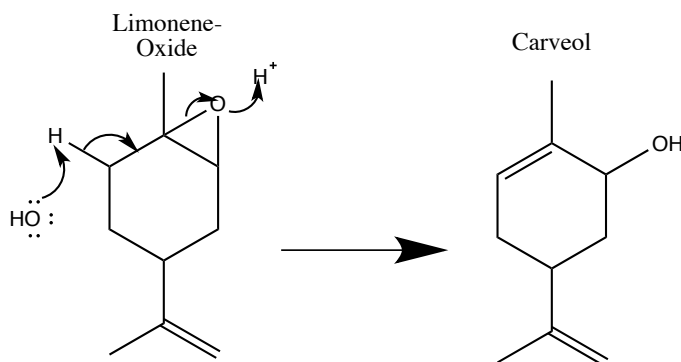


Scheme 6: Loss of the tertiary alcohol from limonene-glycol results in formation of dihydrocarvone through an unknown mechanism. Isotopically labeled water was observed on the product's MS.

Following formation of limonene-glycol, we proposed a secondary product of dihydrocarvone. This species was identified in a variety of samples, but always at low yield (less than 4% of total products). The mechanism is unknown, but we predict that a loss of one water molecule, from the tertiary alcohol in limonene-glycol, resulted in ketone formation alpha to the methyl group (**Scheme 6**). Comparison of the labeled reaction with the reaction on Arizona Test Dust without nitric acid yielded a product peak at about the same retention time in the GC, and an almost identical fragmentation pattern. These two similarities allowed us to conclude that we had isolated the same product, and use of the NIST library showed similarities with a standard MS fragmentation. The O^{18} dihydrocarvone did show a significant peak at the molecular ion, 154 amu, which was two mass units greater than the product in the reaction under normal conditions. The presence of a labeled peak does not confirm our proposed mechanism, but it supports the formation of a ketone after loss of the unlabeled tertiary alcohol on limonene-glycol. The labeled product also indicates that the water may attack preferentially alpha to the methyl group on limonene oxide. Fragmentation patterns of limonene glycol were unable to support preferential attack at either side of the epoxide, so

dihydrocarvone may provide a clue as to exactly how the mechanism of glycol formation occurs.

3.1.3 Carveol as an alternative product to the glycol from the oxide intermediate



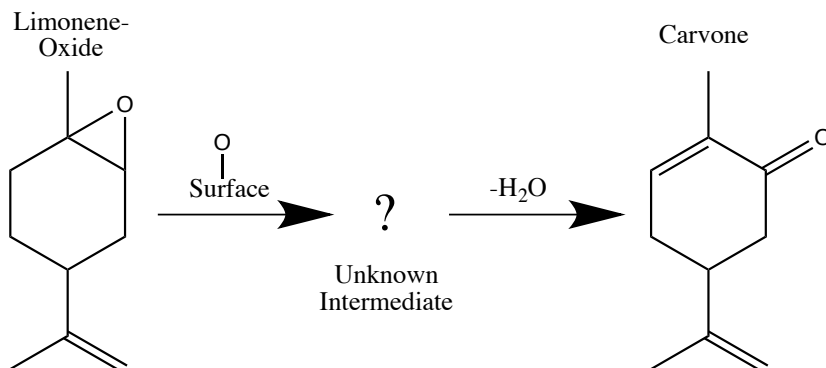
Scheme 7: Proposed mechanism for the rearrangement of limonene oxide resulting in the formation of carveol.

Carveol, which forms a significant portion of the product distributions for alumina without HNO_3 , is a potential less favored product from the epoxide intermediate. We propose that it forms through a rearrangement of the epoxide ring to regenerate an alkene and an alcohol group (**Scheme 7**). This rearrangement would decrease the angular strain of the triangular epoxide, making it more favorable than the epoxide intermediate. This is justified by the greater percentage of carveol than limonene-oxide in all reactions where it was detected, and no carveol where there was no limonene-oxide present. The latter justification additionally supports limonene-glycol as the more favorable pathway from the intermediate. Product distribution in the aluminum oxide reactions without nitric acid indicate that carveol may be formed as favorably as the glycol, so different surface sites may be active in these reactions.

The surface site that may possibly be implicated in this reaction is a Brønsted basic site on Al-OH , which yields Al^+ and OH^- . The reason we hypothesize that the site is associated with alumina centers is that the carveol product is primarily observed in reactions with alpha and gamma phases Al_2O_3 . Once acid is added to these surfaces, the percentage of carveol

composing total product decreases by almost an order of magnitude (from 32.7% to 6.4% in α -Al₂O₃ and 53.3% to 5.5% in γ -Al₂O₃) because the acid likely reacts with the OH⁻ groups and they are no longer as available. On clays, primarily kaolinite, and on SiO₂, these products form in small amounts, if at all.

3.1.4 Carvone: A major product on alumina with an unknown mechanism



Scheme 8: Formation of Carvone from limonene oxide through an unknown mechanism requiring surface sites and loss of water.

The formation of one of the next major products, which dominates in both α and γ phase alumina, is carvone. We hypothesize that this species derives from the epoxide intermediate, but the complete mechanism is unknown (**Scheme 8**). A second reaction with superficial reactive oxygen species following the epoxide formation generates an unknown oxidized intermediate. Removal of water from this unknown intermediate regenerates the double bond within the limonene ring, and leaves a ketone α to the methyl and the reformed unsaturation. There are only two possible locations for the new double bond: on the ring-methyl bond, or within the ring at the base of the methyl bond. We did not have enough data to support preferential unsaturation at one location over another.

In an attempt to clarify the mechanism of carvone formation, we hypothesized that a control reaction without molecular oxygen gas would prevent surface oxygen species from

being regenerated. This hypothesis assumed that both reaction steps using surface oxygen occurred at the same redox site. Our hypothesis was disproven by the detection of carvone in the N₂ gas and ¹⁸OH₂ labeling experiment. The implication of this is that the second surface oxygen reaction must occur at a different site, or through a different mechanism. Also, in comparison with a standard for carvone fragmentation, it can be concluded that the labeling experiment did not cause carvone to be labeled (**Figure 21**). **Figure 21a** displays the raw mass spectrum for both the labeled experiment and a carvone standard, excluding noise peaks about 160 amu. The molecular weight of carvone is about 150 amu, and the same small peaks at high masses occurred both in a standard and in the experiment, so they were excluded as noise. To confirm that the fragmentation was the same, the peak heights were normalized to the reaction product intensity, and the standard was made negative to allow a side-by-side comparison of the peaks (**Figure 21b**). All peaks in the carvone from the reaction corresponded to peaks in the carvone standard, and the intensity pattern was mirrored between the two data sets. This finding provides some support for our proposed mechanism, as it shows that surface adsorbed water neither acts to regenerate surface sites nor does it react to form carvone, and it adds confirmation that we did successfully isolate carvone.

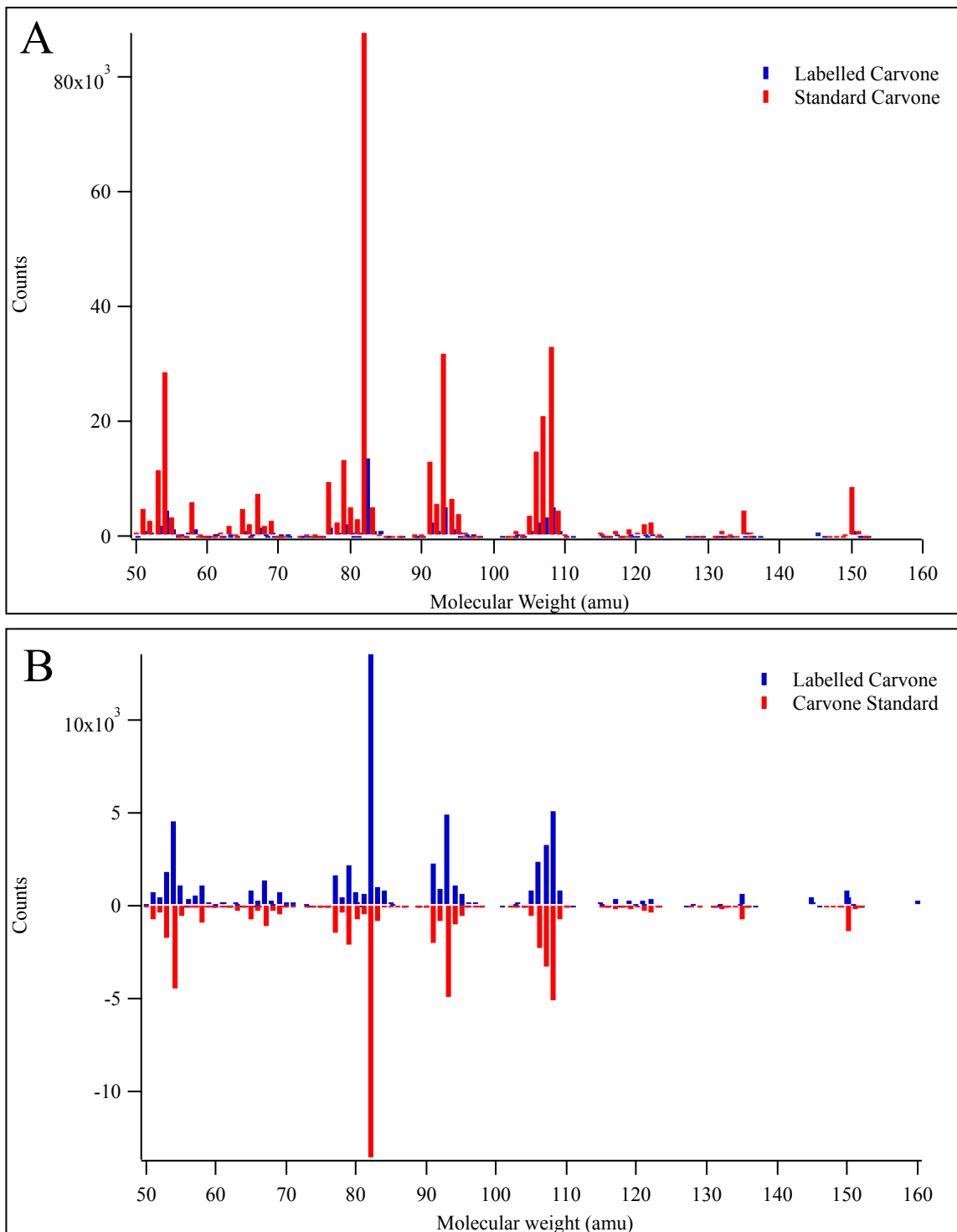
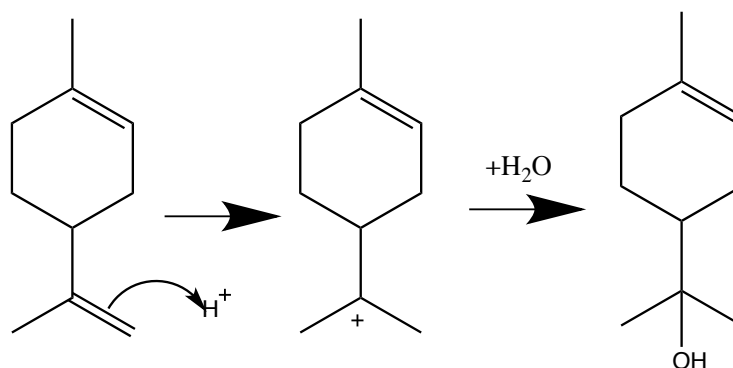


Figure 21: Comparison of the carvone mass spectrum from the labeled reaction on Arizona Test Dust and a standard. Overlap between peaks confirms successful identification of the product. A) Comparison of the raw data, where the standard occurred at much greater intensity to the product. B) The standard was normalized and made negative, so the overlap can be more easily observed, and no shift is observed in the labeled reaction, so the single oxygen atom must come from the surface of the dust.

3.1.5 Terpineol: The expected product from acid catalysis



Scheme 9: Mechanism of acid catalyzed hydration of limonene to terpineol, which is favored at Brønsted acid sites

Terpineol was a product previously reported in literature with a known acid catalyzed mechanism³⁵. We had originally expected to see this as the major product due to the simplicity and well-known nature of acid catalyzed hydration of a double bond. Our data showed the opposite of this expectation, with terpineol occurring as a minor product in only some of the reactions and not occurring in measurable amounts in any others. Formation of a secondary carbocation due to reaction of superficial water with the exo double bond, and attack from a second water molecule caused the formation of a tertiary alcohol at the base of limonene and left the endo double bond intact. The H₂O¹⁸ labeling experiment showed a shift in the peak corresponding to the terpineol after fragmentation of a methyl group at 139 amu, and two small peaks corresponding to fragments containing the alcohol at 71 and 59 amu. Presence of the labeled oxygen confirms the addition of surface adsorbed water, but the unlike with the oxide intermediate the carbocation intermediate is too unstable and therefore was not isolated in our reaction. **Scheme 9** shows this mechanism. Terpineol was found in small amounts in α - and γ -Al₂O₃, but it was found at greater than 15% of total product in Montmorillonite in normal conditions and SiO₂ with adsorbed HNO₃. This trend indicates that terpineol formation is favored when Lewis acid sites are available. Montmorillonite retained some terpineol

formation when reacted in nitric acid conditions, but there was a greater than two-fold decrease in percentage, indicating that the acid affected its Lewis sites. Terpeneol is present in low amounts likely due to favorable hydration of the endo double bond (as seen in all other products) as opposed to the exo double bond hydration. Favorable endo reactions in limonene have precedent in literature, so the low concentrations of terpeneol are consistent with these prior observations^{29,31}.

3.1.6 Summary of Product Mechanisms

Table 3 displays all of the products observed in reactions of limonene on mineral dusts in addition to their associated reactive sites. We have proposed that products requiring a carbocation intermediate (terpeneol and terpin) must go through a Lewis acid site, which can be an Al⁺ center or adsorbed HNO₃. Both of the epoxide intermediates observed require only redox sites to form because neither of these showed the presence of labeling in the isotopic H₂O¹⁸ experiment, so they only rely on surface-bound oxygen. The only other product without labeling was carveol, and we proposed a rearrangement from limonene-oxide to carveol through an unknown mechanism. This mechanism can only require surface-bound oxygen because the carveol had no O¹⁸ label present in the mass spectrum. After the initial redox site to form the intermediate, we proposed that a Brønsted basic site is the source of the rearrangement. Finally, the other products that derive from the epoxide intermediate must use Brønsted and Redox sites. The redox initially forms the intermediate, but the Brønsted sites allow the addition of a labelled O¹⁸ to the product. The Brønsted sites are all surface based when no nitric acid is present, but with the nitric acid pre-treatment on the dusts it is possible that adsorbed HNO₃ could be a source of the Brønsted site.

Table 3: A Summary of the observed products and their associated reactive sites.

Observed Products	Intermediate	Type of Site
	Carbocation	 Lewis Site
	Epoxide	 Redox Site
	Epoxide-Carveol Rearrangement	 Brønsted Basic (after Redox epoxide forms)
	Epoxide-Addition of Surface H ₂ O	 Brønsted or Redox

3.2 A discussion of the effects of mineral dust structure on product formation

3.2.1 An explanation of oxide reactive sites in relation to products formed.

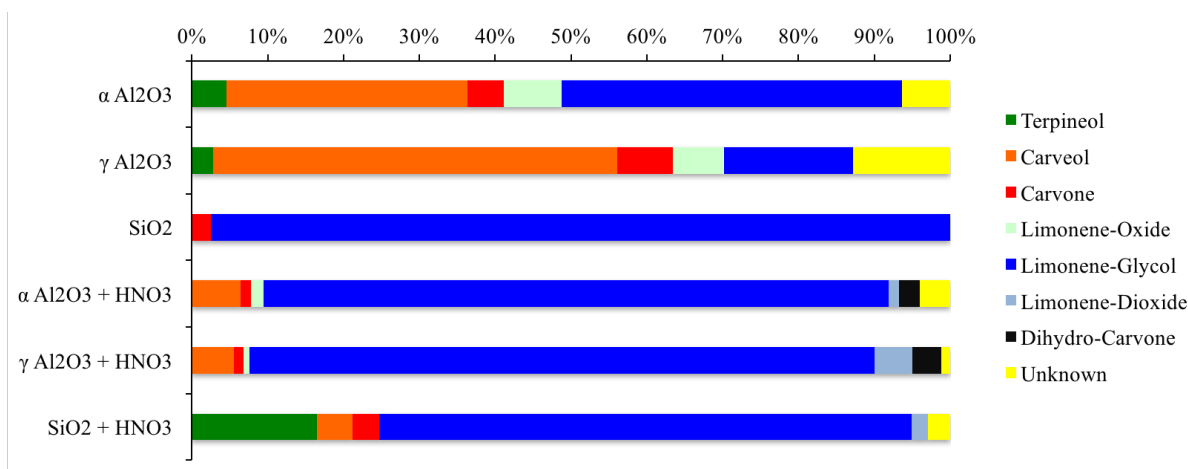


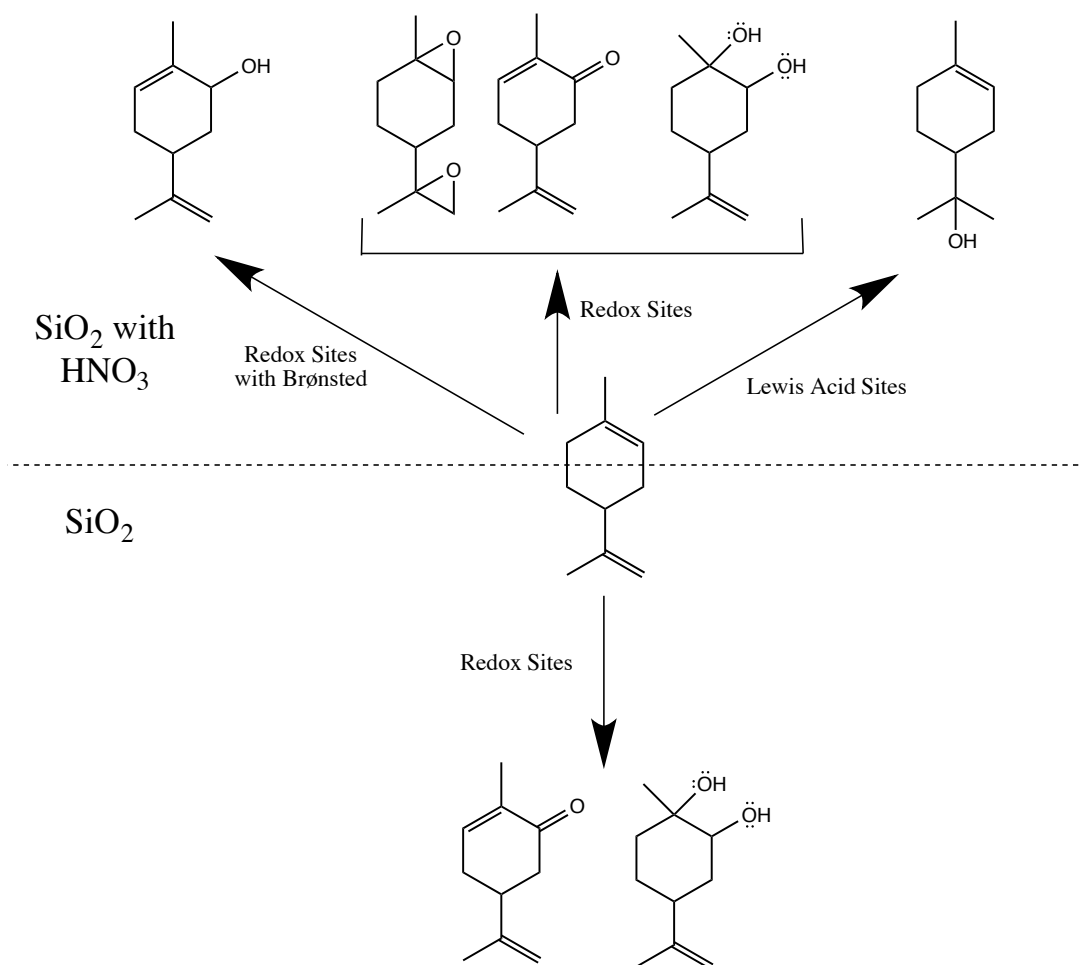
Figure 22: Product distribution for the reactions of limonene on oxide surfaces in conditions with or without HNO₃. The two alumina samples display very similar products, but are significantly different from the silica surface. Products are ordered based on retention time.

Figure 22 shows a product distribution comparison of the three oxides tested where all showed limonene glycol and carvone formation in varying amounts. Both alumina samples,

alpha and gamma, show similar product distributions both with and without nitric acid coating. This similarity indicates analogous surface sites on both samples, likely due to very similar surface structures that only contain aluminum and oxygen atoms. The silica samples, which are pure SiO₂ and lack any aluminum atoms, have a completely different set of surface sites, as is reflected by the different products from reactions on silica as compared to alumina. While silica shows primarily limonene-glycol formation without nitric acid, and retains the glycol as a major product with nitric acid, both alumina samples had lower percentages of limonene glycol formation without nitric acid. Instead, carveol was a major product of the reactions on alpha and gamma alumina. The difference in major products provides further indication for different reactions occurring at alumina and silica bound oxygen species, likely due to the ability of these atoms to catalyze reactions.

The reactions observed on silica without a nitric acid coating all must go through the epoxide intermediate, but after nitric acid coating the silica surface gains the ability to form a carbocation intermediate as evidenced by the presence of terpineol (**Scheme 10**). In the normal reactive conditions, SiO₂ formed only carvone and limonene glycol, which we proposed to form directly from limonene-oxide (see **Scheme 4**) and to be associated with a Redox site. As previously discussed, SiO₂ does not have Lewis sites, and has very weak Brønsted sites so it must primarily rely on Redox. After acid coating limonene glycol remained a major product and terpineol was formed in a significant percentage (16.5%) in addition to small percentages of limonene dioxide, carvone, and carveol. Terpineol was associated with Lewis acidity and carveol may rely on Brønsted sites for rearrangement from the epoxide intermediate, but the other products primarily require Redox sites. SiO₂ converts from primarily reactions using Redox sites into reactions on both Lewis, Brønsted, and Redox sites. Because formation of the

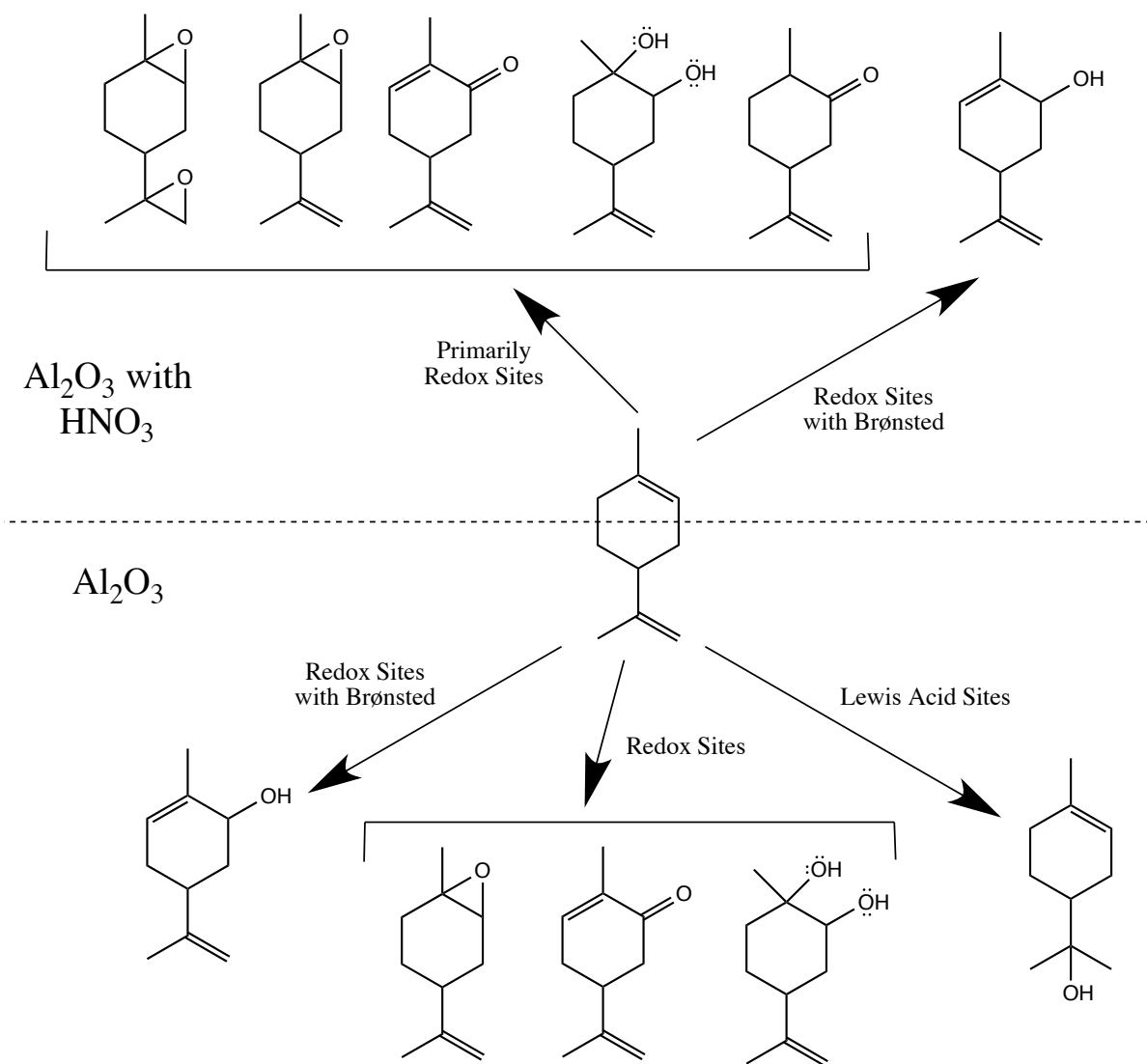
intermediates is linked to the type of site, we can see that the surface of SiO_2 is changing with HNO_3 coating because it now has the ability to act like a Lewis acid.



Scheme 10: Products formed by route of either epoxide intermediates (Redox Sites) or carbocation intermediates (Lewis Sites) on silica. Without nitric acid coating only redox sites are active, but the Lewis sites are also formed after nitric acid coating. Brønsted sites are only clearly implicated in carveol formation.

The pattern on SiO_2 is in direct opposition of the alumina pattern which can go through both types of intermediates prior to nitric acid coating, but loses the ability to form carbocation intermediates after nitric acid pre-treatment (**Scheme 11**). This indicates that Al_2O_3 has all three types of sites with no acid treatment, thus it can use Brønsted and Redox to form carveol and limonene glycol in high percentages in addition to minor products of carvone and limonene oxide, and it can form terpineol on Lewis sites. For Al_2O_3 , the nitric acid removes the Lewis

sites and many Brønsted, so that the primary reactive sites just Redox. The decrease in carvedol percentage is especially indicative of this because while it may be primarily associated the oxide intermediate and thus a Redox site, the rearrangement relies on Brønsted sites, so there must be some available.

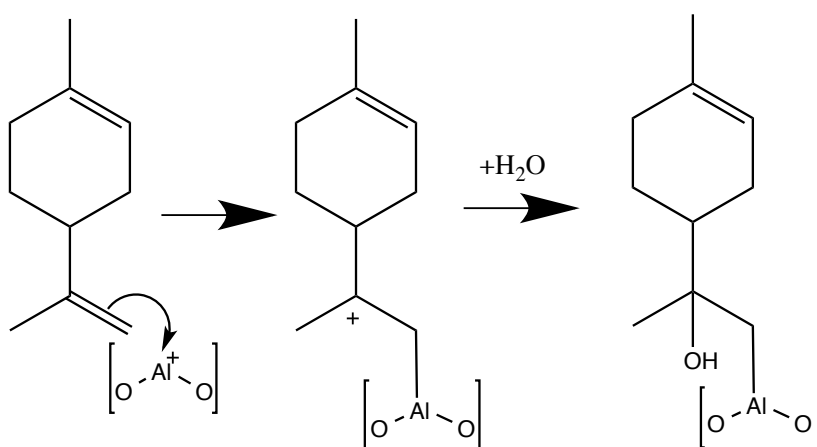


Scheme 11: Products formed on alumina in conditions without nitric acid and with nitric acid. The product distributions demonstrate that the addition of nitric acid removes the majority of Brønsted sites and all Lewis, so all products using the epoxide intermediate and thus the Redox sites are favored in conditions with HNO_3 .

As was discussed in the introduction, Brønsted and Lewis acids and bases show different types of reactivity. Lewis acidity is not usually associated with silica surfaces because of the strong Si-OH covalent bond¹⁶. Lewis acids on mineral surfaces are usually cationic centers, and silica is very electronegative, making it unlikely to form a cation. Alumina is one of the strongest Lewis Acids on metal oxides because of its stability after removal of the hydroxyl group and exposal of the cationic center¹⁶. A similar trend is observed in Brønsted acids, where pure alumina is one of the strongest Brønsted acids of metal oxides, while pure silica is one of the weakest¹⁶. Reactions at the silica site are stabilized by increasing the coordination number of Si through H-bonding with two new water molecules and having a more effective charge distribution on the silicon centers¹⁶. The surface of silica begins in a more acidic state than alumina, where quartz has two reactive silanols with pKa's of 5.6 and 8.5 and pure aluminas have a pKa of 16.6¹⁸. By adding nitric acid to the surfaces, it appears that we are changing the types of acidity. Physisorbed HNO₃ causes increased Lewis acidity, as observed on SiO₂, while reactions with the surface, as observed with Al₂O₃, removes Lewis and Brønsted acidity and may increase the number of redox sites. As seen in **Schemes 10 and 11**, the trends are reversed for silica and alumina with nitric acid coating, and thus we have moved beyond the known acidic properties of each surface.

Though the many types of mineral oxides can catalyze a diverse group of reactions, oxides on metals that only have s and p valence orbitals, such as alumina or silica, generally only show acid-base reactions and routes involving carbocation intermediates¹⁶. In **Scheme 9**, we proposed that terpineol forms through a carbocation intermediate, and this product is only found on alpha and gamma alumina in reactions without HNO₃. Silica-oxygen sites may

lack the ability to form these intermediates, so the ability to form carbocations could be linked to Lewis acidity, which is only present in alumina. This mechanism may act through an Al^+ center acting as the cation to remove the double bond and hold the limonene at the surface, which would then allow attack from H_2O (**Scheme 12**). Both the silica and alumina must have the ability to form the epoxide intermediate, but the alumina sites add favorability to the rearrangement of the epoxide into carveol, while silica clearly favors additional reactions allowing the glycol or carveone to form.



Scheme 12: Formation of terpineol at a Lewis acid site on an Al_2O_3 cationic center.

Coating with HNO_3 provides silica with the acidic surface sites to form carbocations and rearrange limonene oxide to carveol, but this is still a less favored pathway as compared to formation of limonene glycol as demonstrated by glycol remaining the major product on SiO_2 with a nitric acid coating (70.2%). The new ability to form a carbocation intermediate and carveol rearrangement could be due to physisorbed nitric acid acting as a Lewis or Brønsted acid. Nitric acid has the opposite effect on both gamma and alpha alumina by reacting with the surface and removing sites that allow carbocation formation.

3.2.2 An Explanation of Clays

The surface structure of kaolinite only forms one product with nitric acid adsorption and two products in non-acidic conditions. This pattern may provide a simplified explanation for the product formation on clays. All aluminosilicate clays contain a layer of tetrahedral silica stacked above octahedral alumina. **Figure 23** shows how clay sheets stack and the variety of different surface sites available, using kaolinite as an example. Montmorillonite and illite are similar to kaolinite in that they contain layers of primarily aluminum, silica, and oxygen, but illite and montmorillonite are triple layered. Redox sites on kaolinite include the Al=O and Si=O edge defect sites which occur when oxygen is bound to only one of one of the mineral centers and is not hydrated. As was previously described by Tazi et al., silica bound oxygen shows greater reactivity and acidity than similar alumina sites in clays¹⁸. For montmorillonite, studies have confirmed that Si-OH species are more reactive than aluminum oxides at the reactive edge sites of dust particles. The pKa of oxidized montmorillonite was modeled as 8.6, and on a reduced surface it was 11.2⁴⁰. Liu et al. also found that water bound to aluminum on edge sites had pKa's of 5.5, but the ion substitutions of the edge sites often replace alumina, so these sites are neither present or active. The montmorillonite bridging Al-O-Si species had very low pKa's of 1.7, so they would likely be deprotonated on the dust surface. The implication of these different measured pKa's is that sites with low values will likely be deprotonated. Based on this data, we can infer that possible edge sites on montmorillonite include Si-OH/ Si-O at equilibrium, and bridging (ion)-O-Si⁴⁰. This shows a strong presence of Lewis acids (unlike on Kaolinite- **Figure 23**) as aluminum cationic centers, but fewer Brønsted acids available due to the loss of some acidic protons on silicon-bound oxygen.

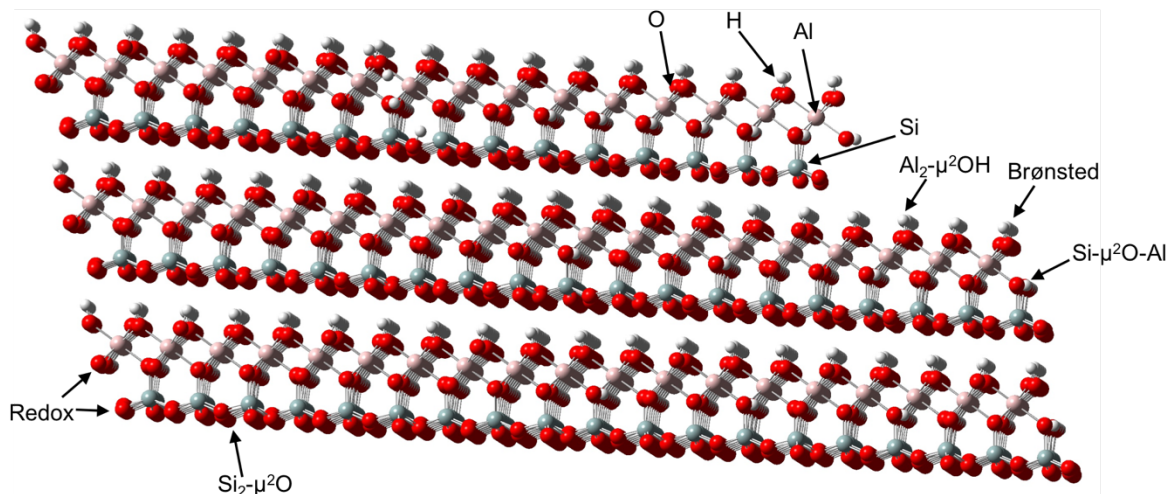


Figure 23: Stacking of kaolinite sheets showing different surface sites and the major reactive sites. Al are pink, Si is grey, O is red, H is white. Silicon-bound oxygen are not hydrated due to their low pK_a^{18} .

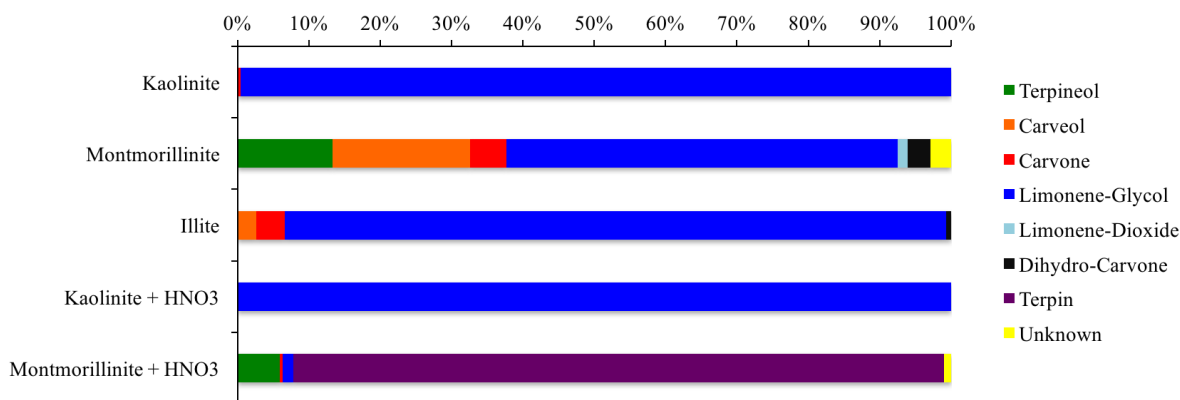
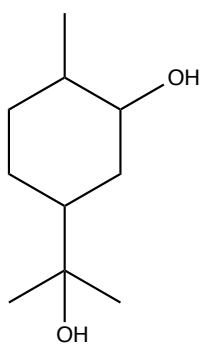


Figure 24: A comparison of the different aluminosilicate clay surfaces used in the heterogeneous reaction of limonene. Products are arranged based on retention time and data yields from Table 1. All reactions showed limonene glycol as the major product, excluding montmorillonite with nitric acid, indicating a different mechanism of product formation occurs. Illite and kaolinite show the most similarity, though kaolinite has only one layer each of tetrahedral silica and octahedral alumina, while illite has three layers of alternating silica and alumina.

Montmorillonite (**Figure 5**) and illite (not pictured), which both contain an additional layer of tetrahedral silica sandwiching the alumina layers and different ions substituted within the layers, have a complicated reactivity due to the variable ionic substitutions. **Figure 24** displays a comparison of the product mixtures for all of the clay reactions, both with and without HNO₃. Illite and kaolinite, which are often found in conjunction in dust storms, show similar reactivity with illite only presenting two additional products as carveol and

dihydrocarvone. The similar product distribution between illite and kaolinite initially suggests a similarity in the reactive sites. If silica were the primary reactive site of the clays, then it might explain their similar products. Illite and montmorillonite have many more silica sites than kaolinite due to the double tetrahedral layer, and even the edge sites would be dominated by reactive oxygen species bound to silica. As previously described, the silica redox sites are much more reactive than alumina's Lewis or redox sites when not coated with nitric acid. When looking at the products formed on kaolinite, similarities can be drawn to the products found on silica. Both showed greater than 97% formation of the glycol product without HNO₃, which confirms the reactive priority of the different reactive oxygens. In a choice between reactions on alumina bound oxygen or silica bound oxygen, the limonene preferentially reacts with silica through an oxidation reaction on acidic sites. HNO₃ coating of alumina did not show the same effect as with silica likely due to the presence of the alumina sites. When nitric acid coating was present, it favored reactions forming limonene-glycol, as was observed on the aluminum-oxide surfaces. This observation provides support for the increase in reactivity of aluminum sites once coated with acid.



Terpin

Figure 25: The terpin product identified as a product of reactions of limonene on montmorillonite with nitric acid coating.

We did not observe the same pattern of reactivity when reacting with montmorillonite or illite. Conditions lacking nitric acid did show preferential glycol formation through the epoxide intermediate on both triple layered clays, so we could deduce that the limonene is likely reacting with the abundant silica-oxygen surfaces on Redox sites primarily. When the montmorillonite surface was coated with nitric acid, a unique product distribution was identified. A previously unidentified terpin product (**Figure 25**) with two alcohol groups attached to both unsaturation sites in limonene was the primary product. As would have been expected based on data from Staniec, this product formed based on an acid catalyzed hydration at both sites³⁵. A carbocation intermediate formed, as with terpineol, but at both sites of unsaturation. The presence of a carbocation intermediate requires a Lewis Acid site, so these must be present on Montmorillonite with HNO₃ coating as either surface Lewis acids of aluminum cations or as physisorbed HNO₃. Clearly, nitric acid coating on a sandwiched surface has a completely different mechanism to any of the simpler systems described. This is perhaps due to interlayer reactivity, but further work to characterize this terpin product and react with similar surfaces, such as illite and nitric acid, would be necessary to deduce any information on it.

3.2.3 Reactions on a mixed surface: Arizona Test Dust

Of the clays and oxides described, Arizona Test Dust in the control condition shows similarity to silica, kaolinite, and illite. All of these models have significant amounts of silica bound reactive oxygens, and as was previously hypothesized, these sites likely take priority in conditions lacking nitric acid. In conditions with nitric acid, Arizona Test Dust still maintains the glycol as its major product, but not to the same extent as kaolinite. Instead, the dust shows more overlap with both to gamma and alpha alumina (with a nitric acid coating)

due to small percentages of carveol and carvone, 3.7% and 2.6% respectively. If more acidic sites are favored in the heterogeneous reactions described, then the control reactions on Arizona Test Dust should show more similarity to surfaces containing large amounts of silica, while the acid coating would cause a lower pKa in the alumina surfaces, and thus a reversal in preferred reactivity. To confirm this hypothesis, it would be necessary to characterize the acidity of sites once they are bound to nitric acid.

Arizona Test Dust, which contained a mixture of different types of clays with SiO₂, calcite, and other carbonates, gave primarily limonene glycol. Unlike the other samples, it showed very little change in product distribution with nitric acid coating. As is shown in **Figure 26**, the only major difference between the two reactions is the presence of limonene dioxide in reaction with HNO₃, and only limonene oxide in the control reaction. Nitric acid likely allowed the reaction to be pushed farther along, as the dioxide product forms from the oxide intermediate through a second reaction with the surface. Due to the variety of surfaces and unknown quantities of different clays in Arizona Test Dust, it is difficult to deduce which surfaces are favored. Additionally, as was previously described, nitric acid may have opposing effects on aluminum and silica surfaces, so in a mixture of both, these opposites may cancel one another out. Without a description of the dust surface sites, predicting reactive mechanisms is challenging, as the product mixtures can only be compared to pure models.

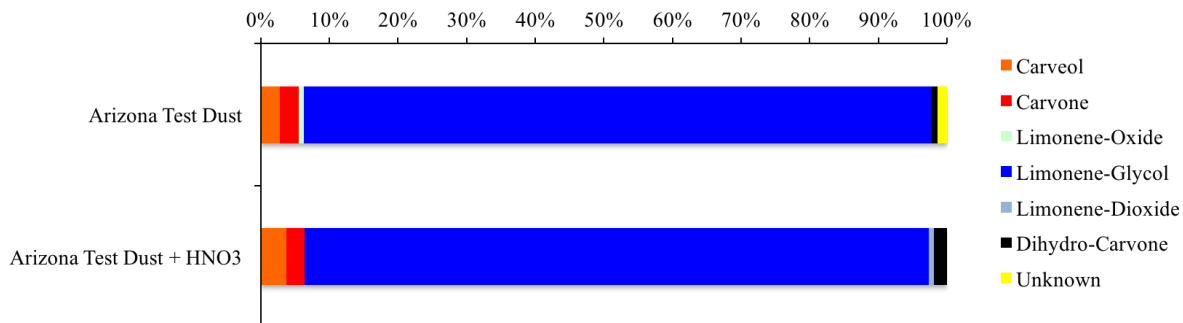


Figure 26: Product distributions for reactions of limonene on Arizona Test Dust in conditions with and without nitric acid. Percentages are based off of data in Table 1 and products are arranged by retention time. No significant change in products is observed, and limonene glycol remains the major product as it composes over 90% of the total products.

Arizona Test Dust provides a summary of the different possible reactive surfaces discussed in this chapter. Conditions without nitric acid lacked products using carbocation intermediates, as opposed to those seen in gamma and alpha alumina, and conditions with nitric acid allowed the glycol-forming pathway to be prioritized over rearrangement to carveol or further reaction to carvone, as opposed to what was observed in pure silica. It is clear that a surface combining silica and alumina would be necessary in a model to accurately demonstrate the variety of reactions occurring in actual dust samples.

Chapter 4: A Kinetic Comparison of Mineral Dusts

To gain a complete understanding of the catalytic mechanisms of product formation on mineral dusts, a study of the kinetics of these reactions is essential. By calculating the reactive uptake of the reactant, limonene, on the different mineral dusts, we can use that figure to compare the reactivity of each surface. Reactive uptake coefficients (γ) were calculated using reactive surface area as measured by a BET, product concentrations, reactant concentrations, and the initial rate of reaction in Equation 3. As previously described, the reactive uptake coefficient can be calculated by a ratio of the number of collisions that produce products to the total number of collisions between limonene and the mineral surface. **Table 4** displays calculated values of surface area, limonene concentration, initial rate, surface collision frequency (Z), and reactive uptake coefficient (γ). **Figure 27** provides a visual display of the reactive uptake coefficients. Patterns of reactivity for the oxides, clays, and mixed mineral dust sample will be discussed.

$$\gamma = \frac{\text{reactive_collisions}}{\text{total_collisions}} = \frac{d[\text{diol}]/dt}{Z}$$

Equation 3

Table 4: Calculated kinetic data for the reactive uptake of limonene on different dust surfaces with or without nitric acid coatings.

	HNO ₃	Total Surface Area (m ²)	[Limonene] (molecules/cm ³)	initial rate (molecules/m ² min)	Z (molecules/m ² min)	γ
α Al ₂ O ₃	No	0.100	1.502E+15	5.300E+15	4.847E+24	1.093E-09
	Yes	0.066	1.503E+15	5.465E+16	4.851E+24	11.26E-09
γ Al ₂ O ₃	No	0.242	1.671E+15	3.507E+15	5.395E+24	0.650E-09
	Yes	0.251	1.392E+15	2.065E+16	4.493E+24	4.597E-09
SiO ₂	No	0.029	1.078E+15	4.370E+15	3.480E+24	1.256E-09
	Yes	0.022	0.846E+15	2.717E+16	2.732E+24	9.946E-09
Kaolinite	No	0.087	1.037E+15	1.970E+16	3.346E+24	5.889E-09
	Yes	0.019	1.411E+15	1.665E+17	4.555E+24	36.56E-09
Montmorillinite	No	0.654	1.513E+15	7.653E+15	4.885E+24	1.567E-09
	Yes	0.314	1.005E+15	8.312E+16	3.244E+24	25.63E-09
Arizona Test Dust	No	0.129	5.322E+15	2.189E+15	1.718E+25	0.127E-09
	Yes	0.134	1.323E+15	4.494E+15	4.271E+24	1.052E-09
Illite	No	0.079	1.458E+15	9.024E+16	4.705E+24	19.18E-09
Calcite	No		1.796E+15			

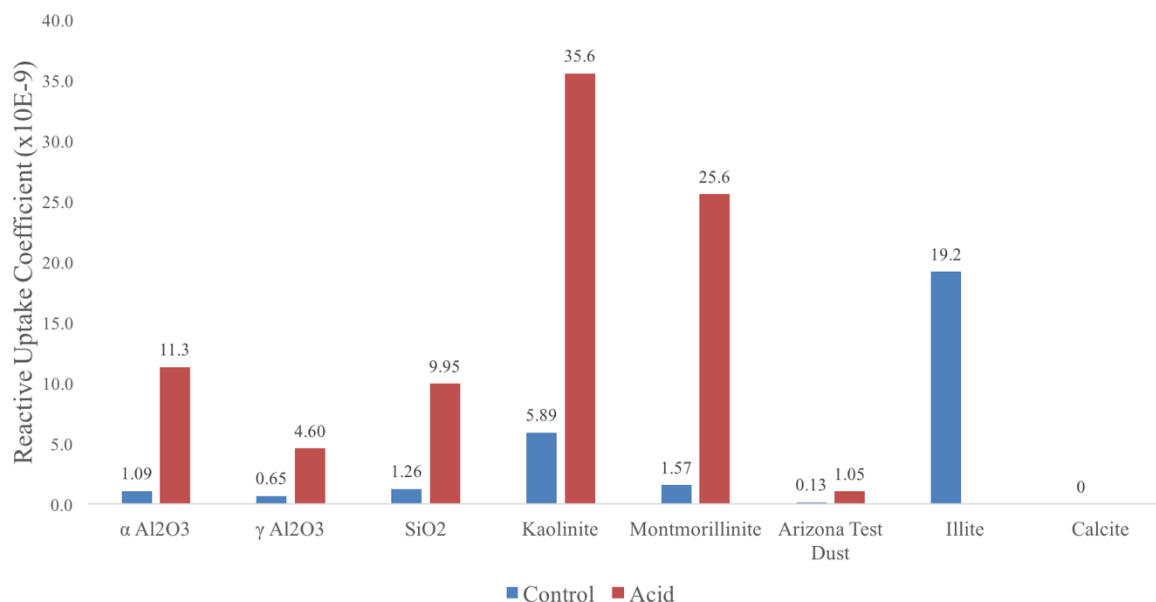


Figure 27: Reactive Uptake Coefficients of limonene on each dust surface ($\times 10^{-9}$)

4.1 Kinetics of Oxides

The three oxides tested were all exposed to relative humidity of about 30% and limonene concentrations ranging from 0.85×10^{15} to 1.1×10^{15} molecules/cm³. To calculate each initial rate, the integrations of the C-H stretching product absorption in the reaction spectra series (**Figure 28**) were calculated. Other peaks identified in these spectra included the loss of surface O-H (3700 cm^{-1}), the growth of metal adsorbed alkenes (1600 cm^{-1}), and the growth of a third unknown absorption (1400 cm^{-1}). There is precedence for an alkene peak occurring at $1600\text{-}1650 \text{ cm}^{-1}$ when adsorbed to a transition metal surface. This peak at 1600 cm^{-1} cannot be due to unbound alkenes because of its strength. We would expect a much weaker peak for alkenes. In this case, we ensured that the alkene peak was occurring only due to surface adsorption by testing the extracted product on an ATR crystal, where this peak was no longer observed. Our finding indicates the 1600 cm^{-1} peak is not related to an unknown or unidentified product, such as a dimer. This peak is solely a result of bonding to the surface, and thus it required no further analysis. The negative peak at 3700 cm^{-1} was not observed in reactions

with SiO₂ and no nitric acid. This peak is likely from loss of OH on the surface of Al₂O₃, and as previously discussed, the Si-OH bond is much stronger than the Al-OH. The difference in strength makes it unsurprising that –OH would be lost on alumina surfaces, and it provides further support for which surface sites were active. Because the negative peak at 3700 cm⁻¹ is found in the oxide reactions that use Brønsted acid sites (Al₂O₃ without HNO₃, Al₂O₃ with HNO₃, SiO₂ with HNO₃), the absorption is due to loss of Brønsted –OH sites on the surface. In reaction spectra recorded with nitric acid coating (**Figure 28**), additional peaks corresponding to the loss of different nitrate species on the surface can be observed.

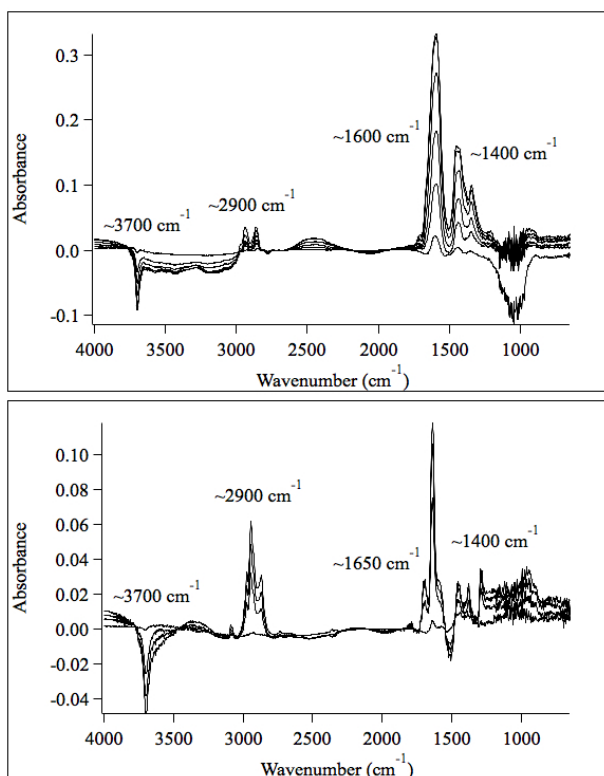


Figure 28: Reaction spectra for the experiments done on alpha phase aluminum oxide with major peaks identified. The top panel displays reaction spectra without nitric acid coating at time points 0, 50, 100, and 200 minutes. The bottom panel displays the experiment with nitric acid coating at times 0, 50, 100, 200, 500, and 1000 minutes.

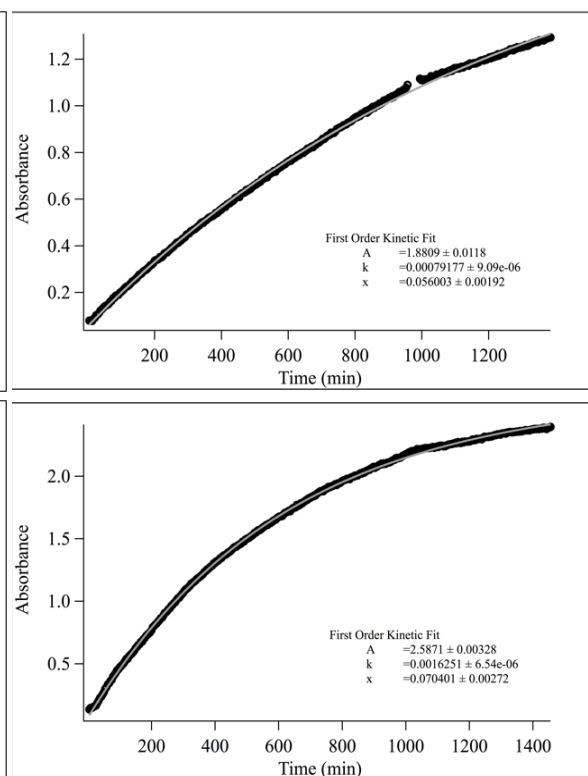


Figure 29: The integrated absorbance of the product C-H stretching peak on a silica surface plotted over time. A first order kinetic fit of the data matches the integration pattern. Panel A is without acid, Panel B is with HNO₃. Data points between 970 and 1000 minutes in Panel A were excluded due to thermal noise.

Integration of the absorbance at 2900 cm^{-1} yielded data that agreed with a first order curved fit line (**Figure 29**). This figure displays the fit using a silica surface with and without nitric acid coating. Successful fit of the data with the curve indicates that the oxides, which all had similar agreement, likely follow a first order mechanism of product formation with respect to surface sites on the dust surface. The fit was based on the equation for product yield: $P(t)=A_0(1-e^{-kt})$, where A_0 is the number of surface sites. Using this assumption, we can deduce that the dust reactive surface sites are used up and filled as the reaction progresses due to decreased volatility of the products and their irreversible absorption onto the dust³⁷. Initially, though, we expect the growth of products to agree with a linear fit due to the large availability of reactive sites. By fitting the first five to ten data points (20-40 minutes) with a line, we were able to calculate the initial rate of each reaction as displayed in **Table 4**. The initial plots had units of absorbance per time, but based on the total amount of products per calculated surface area of the sample, we were able to convert absorbance to molecules/m². This conversion was based on Beer's Law ($\text{Absorbance}=\epsilon\cdot b\cdot c$), though we did not account for path length (b) or absorptivity (ϵ) because these values were the same in all samples. Only the concentration needed to be found to make the conversion to units needed for reactive uptake calculation. The initial rate described the speed of conversion from product to reactant without the time taken for a molecule to search for an open spot. According to the Eley-Rideal mechanism, which limonene has been shown to follow on mineral dusts³⁵, the limonene need not absorb to the surface of the dust; it must collide with reactive sites and previously adsorbed water to initiate a reaction. The Eley-Rideal mechanism states that gaseous species react directly with surface sites or other surface adsorbed species, as opposed to the gaseous species adsorbing prior to reacting. As the reaction progresses and more product adsorbs to the surface of the dusts, fewer

sites will be available, making the correct orientation of collisions a likely rate-limiting step. Due to the lower volatility of the products, they are less likely than limonene to dissociate from the surface as aerosol and they remain on the dust to occupy reactive sites.

Calculation of the total reactive collisions (Z), which was the denominator of the reactive uptake calculation (**Equation 3**) determined by the kinetic theory of gases, allowed us to determine the reactive uptake coefficient on each dust surface. This calculation was performed using **Equation 4**, with concentration of limonene as the only experimental variable. As can be seen in **Table 4**, the fraction of collisions resulting in a reaction, γ , increased by a factor of 10.3, 7.07, and 7.92 for α -Al₂O₃, γ -Al₂O₃, and SiO₂, respectively, due to nitric acid coating. The significant increase in rate indicates catalysis due to nitric acid coating common to all oxide surfaces tested.

$$Z = \frac{[\text{limonene}]}{4} \sqrt{\frac{8RT}{\pi M_{\text{diol}}}}$$

Equation 4

The silica oxide dust surface had a slightly greater reactive uptake, 1.26×10^{-9} , than both gamma and alpha alumina oxide, 0.659×10^{-9} and 1.09×10^{-9} respectively, prior to nitric acid coating. This trend was in agreement with data reported on the reactivity and acidity of silica-bound reactive oxygen species^{18,41,42}, thus providing additional support for the proposed mechanisms favoring Si-O reactive sites prior to nitric acid coating. After nitric acid exposure, alpha alumina became the most reactive surface with a reactive uptake coefficient of 1.13×10^{-8} , which indicates that nitric acid allows some alumina-bound reactive oxygen species to increase in acidity and surface concentration, and therefore reactivity. This increase in alumina reactivity at a greater factor than silica is again in agreement with proposed mechanisms

showing the favorability of alumina reactive sites in clays due to nitric acid coating. Though gamma alumina remains the least reactive of the pure oxides, it increases by a factor of 7.07, which differs from silica's factor by only 0.85, which may be within a margin of error.

Nitric acid appears to have a greater effect on alumina sites in pure Al_2O_3 than on silica sites in pure SiO_2 , which should have interesting consequences for mixed aluminosilicate surfaces based on their exposed reactive sites.

4.2 Kinetics of Clays

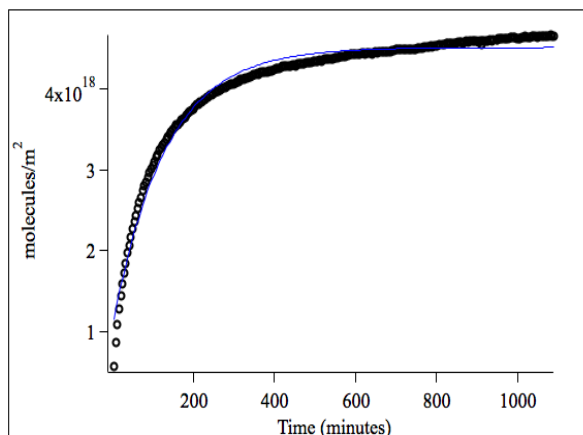
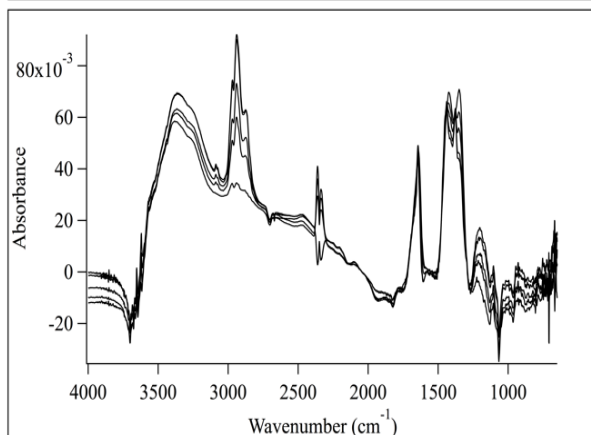
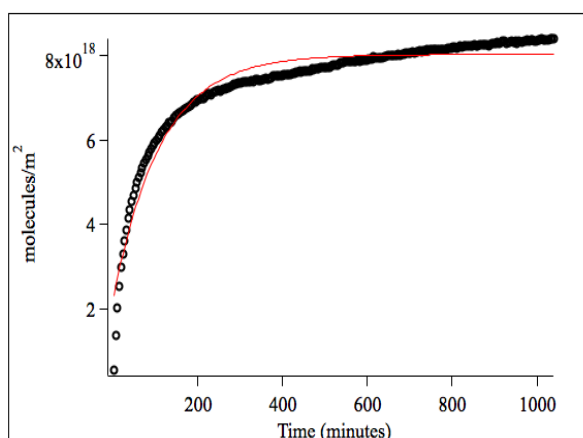
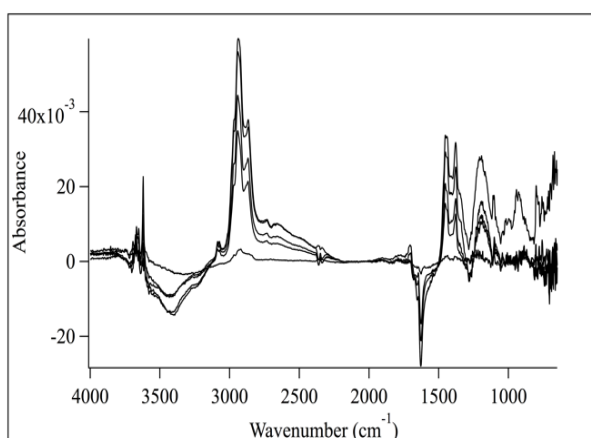


Figure 30: Reaction series spectra for experiments on kaolinite with (bottom) and without (top) nitric acid. Time-points are 0, 50, 100, 500, and 1000 minutes. The characteristic product peak appears in both spectra at $\sim 2900 \text{ cm}^{-1}$ and a difference in the lower wavenumber absorptions corresponds to nitric acid derived species present in the bottom panel.

Figure 31: Integrated product peaks over time for reactions on kaolinite in control (top) and nitric acid coated conditions (bottom). Both follow first order kinetic fits, indicating that the clay surfaces maintain a first order mechanism of reaction with limonene.

Similar to reactions with pure oxides, limonene concentrations remained within range at 1.0 to 1.5×10^{15} molecules/cm³ and relative humidity remained at about 30% for reactions with kaolinite, montmorillonite, and illite. Both kaolinite and montmorillonite were tested with nitric acid, but illite was not due to time constraints and technical difficulties. Series of reaction spectra were collected and integrated, as displayed by an example on kaolinite in **Figure 30**, where similar IR absorptions were recorded, excluding the large peaks at 1650 cm^{-1} found on both alumina dusts. Again, first order fits were applied to all of the series as shown for kaolinite in **Figure 31**, which acts as confirmation of the retained mechanisms on silica and alumina bound oxygen species. After linear fit of the first data points in each series, Z and γ were calculated to compare reactivity. Illite had the greatest γ of the clays at 19.2×10^{-9} , which was an order of magnitude greater than montmorillonite, 1.57×10^{-9} , and was greater than double the value for kaolinite, 5.89×10^{-9} . Additionally, illite without nitric acid coating was nearly as reactive as both other clays with acid, indicating that the additional silica layer may have provided increased reactivity over the double layer in kaolinite. Nitric acid did significantly increase the reactivity of both the kaolinite and montmorillonite surfaces by factors of 6.21 and 16.4 respectively. Likely the inserted ions, specifically Calcium ions, allowed montmorillonite to be much less reactive than both the kaolinite and illite surfaces, but much more affected by nitric acid coating. The presence of the ions themselves affects the reactivity because they can act as a more reactive Lewis acid cationic site. CaCO_3 was not reactive, likely due to the instability of a C^+ forming from the reduction of the mineral surface during oxidation reactions with limonene. The large difference in reactivity on montmorillonite agrees with the major differences in product distribution from both the other clays and the oxides. Montmorillonite was the only surface that formed terpin, and it needed Lewis sites to perform this reaction, and

Lewis sites on aluminum cations were shown to be much less reactive than the silicon-bound Redox sites.

All of the clays, interestingly, showed much greater reactivity than the pure oxides. This may be due to the greater variety of surface sites available, or it could be due to the different properties of mixed aluminosilicates. Due to the high percentage of limonene glycol produced on the dusts, ease of producing the glycol on clay surface sites may also be related to the higher activity. Altering the ratio of silica to alumina can also have effects on the products formed and the catalytic reactivity of Brønsted acid sites, and a greater relative amount of alumina can cause more crowding of products on the surface⁴³. Our data for kaolinite and illite agrees with these observations, as illite has a much greater Si/Al ratio, so it should have less crowding and a greater rate of formation. This does not explain the lower reactivity of montmorillonite, which one might expect to have a similar γ to illite due to the triple layer of alternating Si-Al-Si. If the metal ion substitutions in montmorillonite occurred primarily in the tetrahedral silica sites, this would lower the Si/Al ratio in addition to potentially removing reactivity from surface sites, which might explain its lower reactive uptake. If the ion substitutions in illite occurred at alumina sites, this would have much less effect on the highly reactive silicon-based sites because aluminum is sandwiched between two tetrahedral silica layers, and it could increase reactivity by further increasing the Si/Al ratio and decreasing crowding. As previously discussed, the growth of a monolayer over the dust surface limits the available surface sites, so decreasing crowding would allow more sites to be accessible for reactive limonene collision. Without a definite structure of our samples, we were unable to determine what ions were present and in which locations they were substituted.

4.3 Kinetics of a Mixed Dust

Arizona Test Dust, which is likely composed primarily of clays as previously discussed, displayed a reactivity much lower than the clays and oxides tested. After the same procedures were performed to calculate initial rate, Z , and γ , the low values of γ indicated that few collisions resulted in product formation. When studying the IR spectral series for Arizona Test Dust with and without nitric acid (**Figure 32**), we see similar peaks to those described for the clays and oxides, with slight alterations in the lower frequency nitrate ion area. Arizona Test Dust, like all other samples, showed first order reactivity when fit with the equation $P(t)=A_0(1-e^{-kt})$ (**Figure 33**). Coating with nitric acid increased the reactivity by a factor of 8.26, from 0.127×10^{-9} to 1.05×10^{-9} , but even with the added acidity Arizona Test Dust had the lowest reactive uptake coefficient. Only gamma phase alumina had lower reactivity. Acid clearly had a greater effect on Arizona Test Dust as evidenced by comparison of the factors of increased reactivity, but it still displayed a puzzlingly low overall activity considering the wide range of products observed.

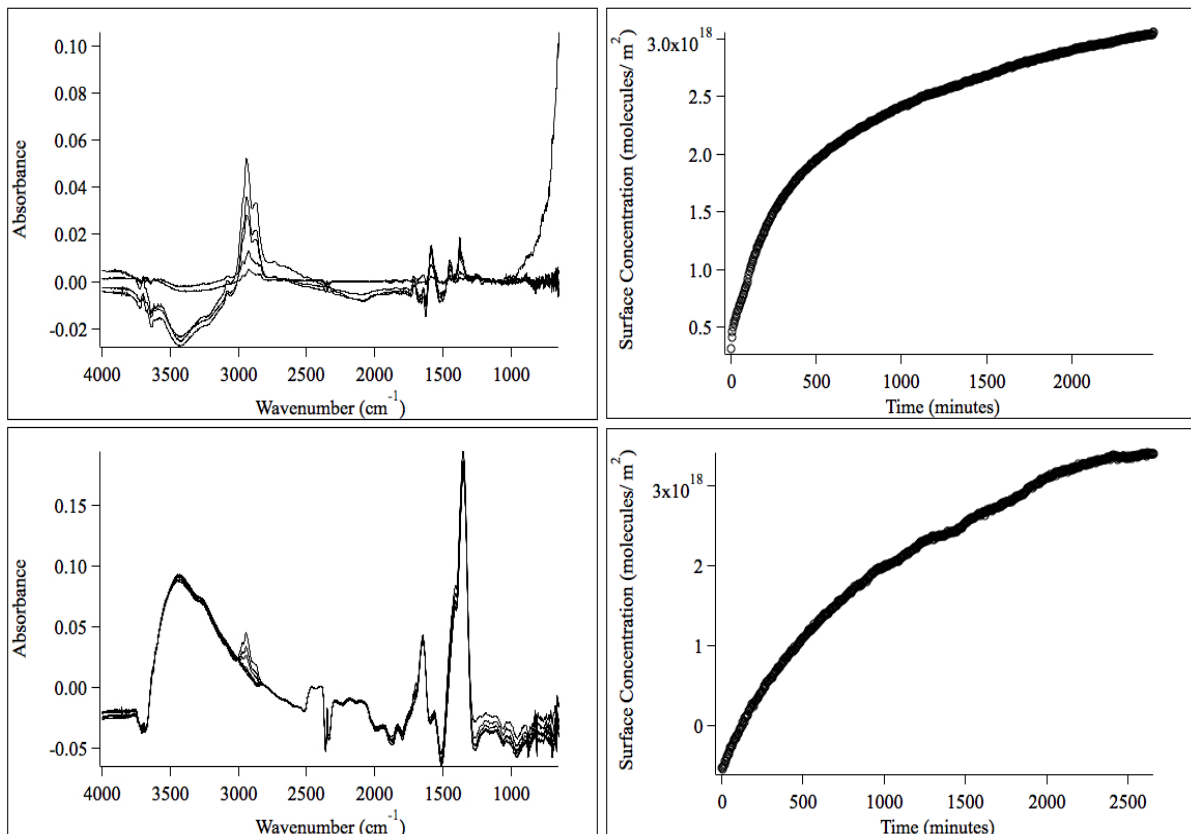


Figure 32: Reaction series spectra for reactions of limonene on Arizona Test Dust in normal conditions (top) and with nitric acid pre-treatment of the dust surface (bottom). Time-points were 0, 50, 100, 500, and 1000, and 2500 minutes. The C-H stretching of the product peak is again observed at ~2900 cm⁻¹.

Figure 33: Integrated product peaks over time for reactions on Arizona Test Dust in control (top) and nitric acid coated conditions (bottom). Both follow first order kinetic fits, indicating that they have the same kinetics as the clays as oxides as previously discussed.

Chemical	% Of Weight	Chemical	% Of Weight
Silicon	69.0 - 77.0	Calcium	2.5 - 5.5
Aluminum	8.0 - 14.0	Magnesium	1.0 - 2.0
Iron	4.0 - 7.0	Titanium	0.0 - 1.0
Sodium	1.0 - 4.0	Potassium	2.0 - 5.0

Table 5: Elemental composition of Arizona Test Dust sample as reported by the supplier.

The lack of reactivity could be explained by the complexity and unknown nature of the dust sample. While the elemental composition shows primarily Silicon composing the sample, aluminum, iron, and calcium all occur in appreciable amounts (**Table 5**). This study focuses on aluminosilicate modeling of atmospheric dusts, but there are additional possibilities of clays

and mineral-oxides found in the atmosphere. Calcite, CaCO_3 , which has been estimated to make up a significant portion of dust storms in the American southwest¹³, was also tested in this study and it yielded no products and we were unable to coat the surface with nitric acid. If a significant portion of our dust sample were composed of calcite, it would dilute the reactivity of the surface, and yield a lower reactive uptake than expected. Additionally, there are further clays and dusts that make up this sample, such as quartz in structures other than our pure SiO_2 sample, that could display different reactivity or no reactivity, and therefore cause a decreased observed reactive uptake. We only used one type of SiO_2 , and because silicon is a major component elementally of the sample, it is likely that there are other configurations of the oxide present, and these may show slightly different reactivity.

4.4 Effects of Acid on Particle Size

One secondary effect not yet discussed is the decrease in BET surface area due to nitric acid coating. This observation holds for all dusts tested and accounts for a small fraction of the increase in reactive uptake coefficient. We hypothesized that the decrease in surface area might occur by one of two mechanisms: it could be due to acid eating away at the surface of the dusts and acting to smooth out any defects, or it could fuse particles together to create larger particles with less exposed surface (**Figure 34**). Pores or holes in the surface might expose more reactive oxygen species for the acid to react with, and these defects of the surface might be removed. Additionally, to confirm that the acid was not acting to decrease the surface area by fusing dust particles together and exposing less surface sites, we used a Tornado DPS system to determine the particle size. As seen in **Figure 35** the percentage of particles with a smaller diameter increased after coating samples of silica. Additionally, the mean diameter decreased by almost 50% for SiO_2 from 4.58 μm to 2.95 μm . Had the particles fused with acid, we would have

expected to see an increase in particle size, but the result indicates that we were correct in assuming that acid acts to smooth the surface of all tested dusts.

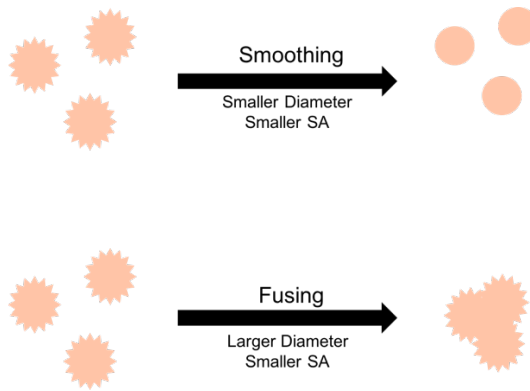


Figure 34: Possible mechanisms for decreasing the surface area of mineral dust particles. By smoothing the surface with nitric acid, the diameter of particles would decrease. Fusing the particles with nitric acid would cause less of the surface of each particle to be exposed, but the diameter would increase with a greater number of particles being grouped into an irregular shape.

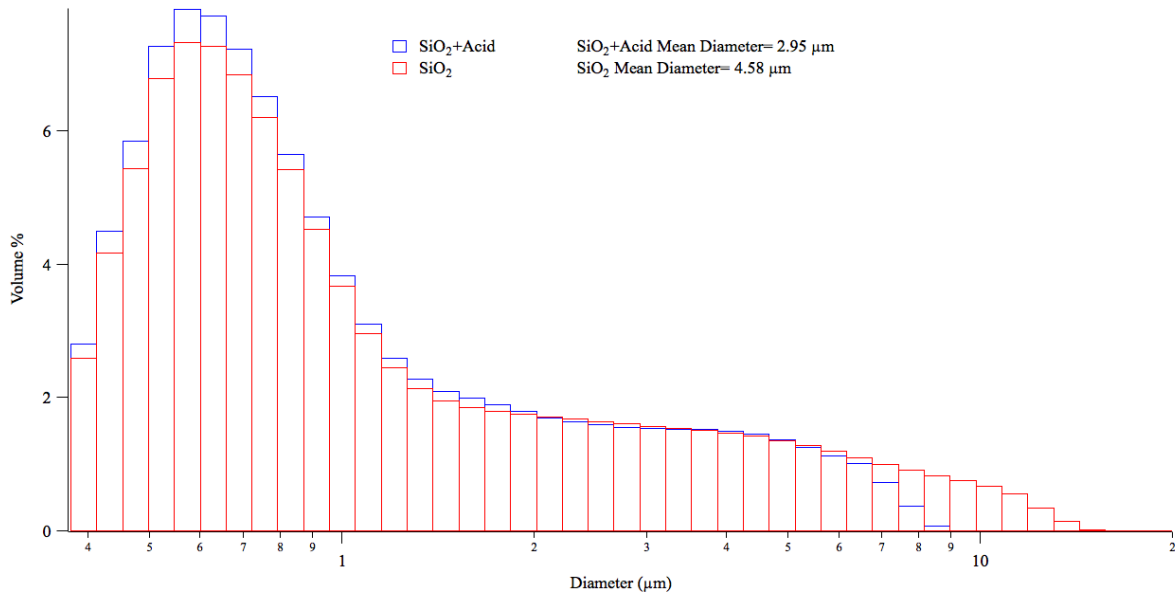
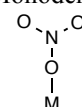
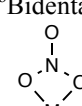
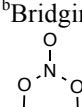


Figure 35: The volume percentage of particles at different diameters as observed by a Tornado DPS system. Nitric acid coating of the silica particles caused a shift in percentages towards lower diameters. Due to smaller particles being less affected by gravitational settling, it is likely that the nitric acid coating allows particles to remain suspended in storms and clouds for a longer period of time.

The surface areas of α - Al_2O_3 , γ - Al_2O_3 , and SiO_2 decreased by factors of 1.5, 1.0, and 2.6 respectively. In comparing the effect of HNO_3 on both phases of Al_2O_3 , alpha phase was affected to a greater extent than gamma; this trend remains in agreement with the effect of

HNO₃ on the reactive uptake on each alumina dust. The gamma phase appears to be unaffected by nitric acid coating, which may be due to error in measurement or it could be caused by the acid acting in a different mechanism on this surface. Further studies and duplicate measurements would be needed to understand how HNO₃ affects the particle size and surface area of gamma phase alumina. Interestingly, SiO₂ is affected much more than either alumina structure, in terms of surface area, while it is affected less than alpha alumina in terms of reactive uptake. This is likely due to the different acidity of each surface prior to coating. SiO₂ is acidic prior to coating, so it must have fewer basic sites for the HNO₃ to react with than either of the less acidic alumina surfaces. This is reflected in the nitrate species observed on each of the dusts, which were identified based on nitrate ion absorptions previously reported in literature. **Table 6** displays all observed nitrate ion peaks on the samples, but the presence of large product peaks present in both reactions with and without nitric acid obscured the locations of some peaks. There is a possibility that these peaks still exist but are hidden within the larger product peaks, but based on the size and reactivity effects it is likely that the alpha phase alumina contains more nitrate species, accounting for the greater impact of acid on the surface. Both reactions with alumina had surface adsorbed HNO₃ present, which could account for their increased acidity, while silica only displayed nitrate peaks, which would have acted to decrease acidity, and potentially reactivity. The highly acidic silica surface did react with most of the HNO₃, while a significant amount remained on the more basic alumina surfaces.

Table 6: Observed peaks in reaction spectra corresponding to nitric acid-derived species.

Nitrate Ion	α Al ₂ O ₃	γ Al ₂ O ₃	SiO ₂	kaolinite	montmorillonite	Arizona Test Dust
^a surface adsorbed HNO ₃	1673	1670		1687		1687
^b Monodentate 	1565		1558	1540	1540	
^b Bidentate 	1580			1575		
^b Bridging 	1624	1630				
^b Solvated NO ₃ ⁻	1417	1416	1419	1425		1421

^a Based on reported absorptions from Angelini et al. ^b Based on reported absorptions by Underwood et al.

The clay surfaces also exhibited a decrease in surface area and particle size due to nitric acid coating, where kaolinite decreased by a factor of 3.7 and montmorillonite decreased by a factor of 1.8. Due to kaolinite's different exposed surfaces, the homogeneous model of atmospheric storms and the common laboratory assumption that alumina and silica together equal clays predicted that the size difference would be an intermediate of the pure alumina and silica. Instead, the clay showed a decrease in surface area much larger than any of the oxides, further showing that this assumption that oxides react in the same way as clays is flawed. It is possible that a clay, which is multilayered, could have more defects in the surface than a purified oxide, which might be the cause for the greater smoothing of the surface. Were this assumption true, though, then a clay with more layers or more silica layers should have the greatest effect due to nitric acid. If the previously discussed hypothesis about preferential silica substitution in montmorillonite were true, then this could also explain the decreased effect of

nitric acid on particle size for the sandwiched montmorillonite clay. **Table 6** shows identified nitrate ion peaks for the clays and Arizona Test Dust. Of the observed nitrate absorptions, we may come to the conclusion that due to the increased number of nitric acid derived species on the surface of kaolinite allows for nitric acid to have a greater effect on the reactivity and size. This supports the previous discussion on nitric acid derived species observed on the oxide dusts. Arizona Test Dust, which had more absorptions than montmorillonite was less affected by the nitric acid coating in terms of BET surface area, which only decreased by a factor of 1.4. The small decrease in surface area could be attributed to the complexity of the surface due to the presence of additional dusts. As was previously discussed, some clays which are not reactive in these conditions, such as calcite, might dilute the reactivity, or in this case the ability of acid to react with the surface.

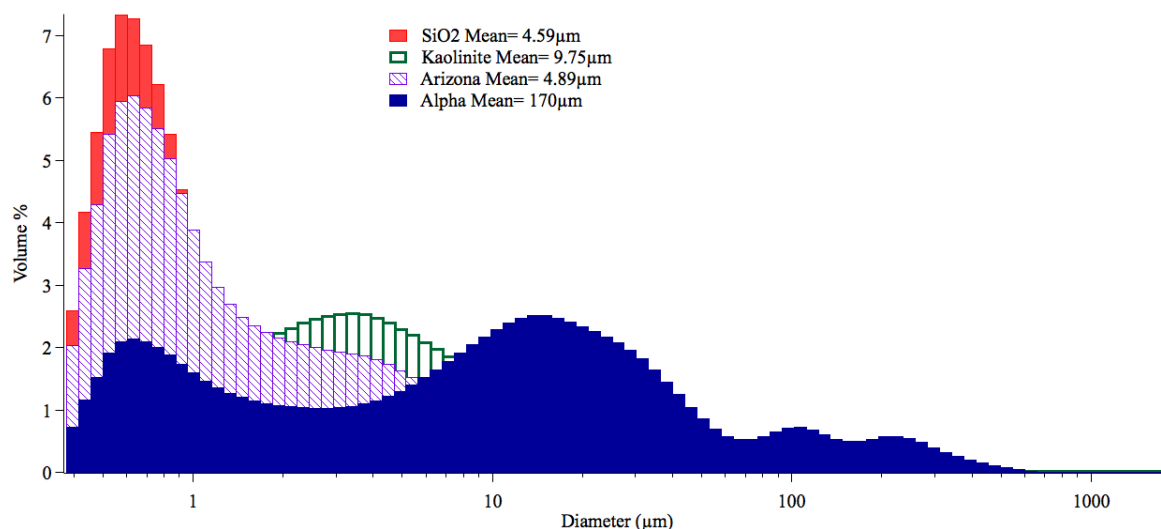


Figure 36: The mean diameters of four dust samples without nitric acid coating. Arizona Test Dust, kaolinite, and silica all fell within the diameters of observed particles in dust storms (Blanco, Geng), making them the most atmospherically relevant and likely to react. Alpha-alumina had a large mean diameter at 170 microns, making it unlikely to be very relevant for long range transport in dust storms and clouds.

A final factor to consider is the consequence of altered particle size on the lifetime of different dusts. A variety of sources cite particle diameters between 0.3 and 30 microns⁸ or 0.5

to 16 microns¹⁵ as the most commonly observed in long range transport, clarifying that the smallest particles are transported most effectively. As shown in **Figure 36**, the alumina oxides displayed a large diameter, with the mean diameter calculated as 170 μ m for alpha alumina prior to nitric acid coating, while silica, kaolinite, and Arizona Test Dust all had mean diameters below 10 microns. The most relevant particles are reported to have diameters less than 1 μ m⁸, which is approached by the clays, silica, and Arizona Test Dust. By decreasing particle diameter and surface areas using nitric acid, the particles are becoming both more reactive and more easily transported. Not only are they more likely to react, but these particles will be present for a longer period of time, thus extending their impact on the atmosphere.

In summary, the clays were the most reactive group, and Arizona Test Dust, which is composed of a variety of minerals and clays was the least reactive sample. The high clay reactivity and the large difference in particle size changes as compared to the pure oxides provides support for the idea that a homogenous model of the atmosphere is not accurate. Additionally, the mixed dust, which contains a number of other untested minerals and particles did not react at a rate on the order of any other dust sample, so use of pure oxides as the only model for dust storms is flawed. Nitric acid had a much larger effect on montmorillonite than on kaolinite in terms of reactivity, and it affected alpha alumina more than any of the other oxides, thus furthering the divide between clay and oxide reactivity. The differences in clay structure are the most likely causes for inconsistent reactivity between samples. The pure oxides, which only contain one type of structure, differ greatly from clays which can have stacked layers of tetrahedral silica and octahedral alumina, as in kaolinite, or sandwiched layers with an additional silica layer below the alumina, as in montmorillonite and illite (**Figure 37**). The latter triple-layered clays can also have various ionic substitutions, which may account for

the difference in reactive uptake coefficients for montmorillonite and illite. Substitution of silica atoms in montmorillonite and alumina atoms in illite could cause the activity on illite to increase, while montmorillonite would decrease due to the effects of crowding and lack of reactive acidic sites. Additionally, nitric acid has been consistently shown to have a strong catalytic effect on all of the samples, but the trends observed from product identification and mechanisms are conserved.

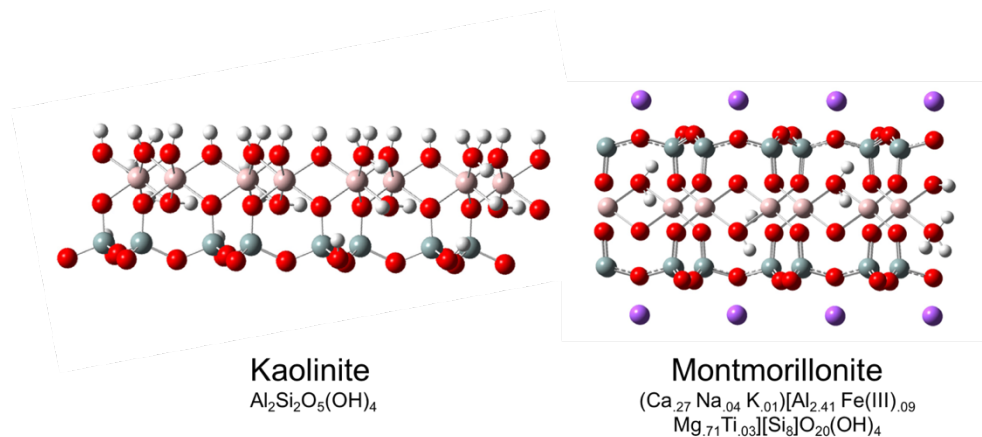


Figure 37: Structures of the two clay samples that were tested with HNO_3 pre-treatment. Both likely produced different nitrate derived species that acted as different types of acids in the reactions.

5. Conclusions

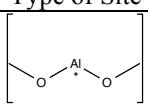
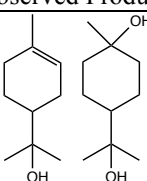
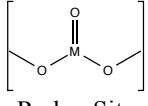
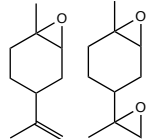
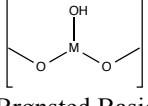
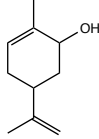
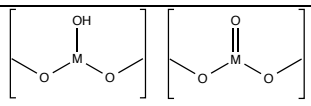
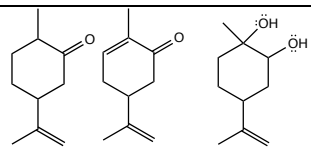
5.1 A Summary of the Results

In a study of the products of heterogeneous reactions of limonene on mineral dusts, we found that both the mechanism of reaction and the reaction kinetics differ between clays and oxides. Limonene, which has a lifetime between 40 and 80 minutes, is an atmospherically relevant model for reactive VOCs. Though it has a relatively short lifetime, there is a large quantity of limonene available in the atmosphere, so its concentration remains constant throughout the reaction. The limiting reactant in these reactions is the aging dust as it falls out of storms due to gravitational settling. The focus of this study was the differential reactivity of the dusts and evaluating the validity the current model of SiO₂ and Al₂O₃ reactivity adding to give the reactivity of aluminosilicate slays.

Oxides have been the primary laboratory model for reactions of trace gases on mineral surfaces in the atmosphere, but due to different surfaces found in pure oxides (specifically Lewis sites) as opposed to mixed aluminosilicate clays, we observed different reactions occurring. In conditions lacking nitric acid, silica-bound oxygen were likely the most reactive sites on the surface of dusts. **Table 7** shows these as the redox, or Brønsted and Redox, classifications. Kaolinite acted most like silica without nitric acid coating, indicating both of these have primarily active redox and Brønsted sites, but they lack Lewis acid reactivity. Kaolinite and silica with acid coating displayed reactivity corresponding to presence of Lewis, Brønsted, and Redox sites, so the nitric acid may have acted more like a Lewis acid on these surfaces. Lewis acid sites had the ability to form carbocation intermediates or they favored reactions allowing rearrangement to carvone from the epoxide intermediate. As Lewis sites became available, they became more favored, accounting for the greater presence of

carbocation-based products in both alumina species, montmorillonite, and silica with nitric acid. Illite did not form carbocation intermediates, so the surface was likely dominated by redox or Brønsted sites. When nitric acid was added to dusts containing Lewis sites (Al_2O_3), the Brønsted-type acidity of the nitric acid dominated, so few carbocations were observed. Montmorillonite is an exception, because it had both Brønsted and Lewis sites available, so it maintained the ability for form both intermediates.

Table 7: Intermediates and products observed for each classification and combination of reactive sites.

Type of Site	Reactions	Intermediate	Observed Products
 Lewis Site	$\alpha\text{-Al}_2\text{O}_3$ $\gamma\text{-Al}_2\text{O}_3$ Montmorillonite Mont+Nitric $\text{SiO}_2\text{+Nitric}$	Carbocation	
 Redox Site	All Dusts	Epoxide	
 Brønsted Basic	$\alpha\text{-Al}_2\text{O}_3$ (with or w/o) $\gamma\text{-Al}_2\text{O}_3$ (with or w/o) Montmorillonite $\text{SiO}_2\text{+Nitric}$ Arizona (with or w/o)	Epoxide-Carveol Rearrangement	
 Brønsted or Redox	All Dusts	Epoxide-Addition of Surface H_2O	

The implications of this different reactivity can be realized when studying the rate of reactions. The most reactive mineral surfaces, which were nitric acid coated clays, had a decreased range of products due to the fast reactions on favored sites. Reaction and regeneration of the acidic sites on these surfaces, as described by Busca, occurs so quickly that the slower, less favored reactions on lower acidity sites occur relatively less, which renders products from these reactions very uncommon or completely undetectable¹⁶.

The nitric acid coatings, which have been shown to occur at a rate faster than can be

measured with our instrumentation³⁷ alter the favorability of different sites in addition to speeding the reactions that occur on them. The oxides were shown to be much more affected by acid coating than the clays (with the exception of montmorillonite), with a greater than 7 factor of increase for all oxides tested. The size change due to nitric acid can be observed in the factor of surface area of decrease on each surface, where the aluminum oxides had factors of 1.51 or less. Only silica-rich surfaces such as kaolinite, montmorillonite, and SiO₂ showed large surface changes due to nitric acid coatings.

The implication of this observation is that the dusts which are most atmospherically relevant are the clays and SiO₂ because of the small diameter. Their reactions occur much more quickly than on the particles with larger diameters, such as α and γ phases Al₂O₃, so they produce much more SOM than the aluminum oxides in the same amount of time. Additionally, based on the size of the different particles, the clays and small oxides remain in dust storms and clouds for a longer period of time and are transported farther than any large oxides. Over deserts, which are the main sources of mineral dust, there is relatively little VOC due to biogenic sources, and as many of these locations are not inhabited, they are not studied extensively for air pollution by anthropogenic VOCs. For reactions with the non-methane trace gases, such as limonene, to occur, the dust must be transported long distances to large cities or highly vegetated areas.

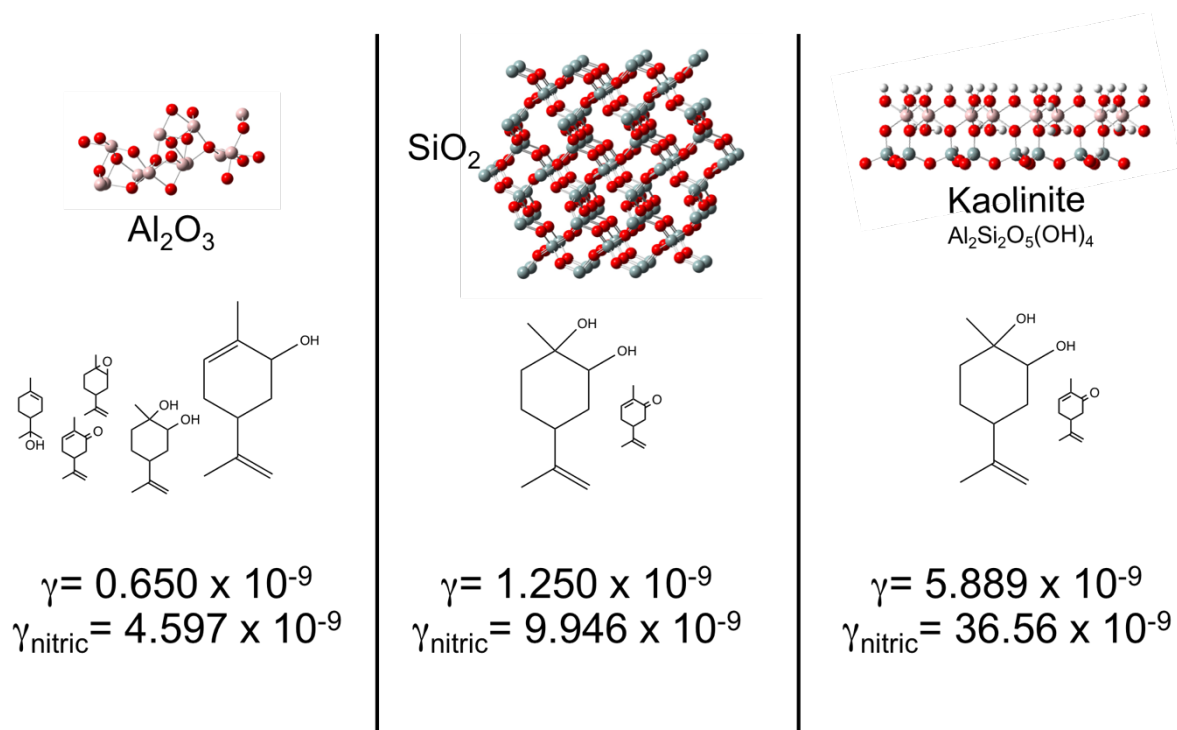


Figure 38: Addition of Al_2O_3 and SiO_2 product distributions and reactive uptake coefficients does not yield the reactivity of kaolinite, which invalidates the current model. Major products are pictured as the largest molecules under each dust type, and the uptake coefficients without and with HNO_3 are both pictured. These clearly do not all correlate as kaolinite has much faster reaction rates and different products than alumina.

These differences in kinetics and product distributions indicate that the current model of modeling mineral surface reactivity is invalid. As shown in **Figure 38**, addition of alumina reactivity with silica reactivity cannot yield what was observed for kaolinite. The major products without acid, as highlighted in **Table 8** are different on γ phase Al_2O_3 than on SiO_2 or on kaolinite. Additionally, the same inability to add products can be observed when the nitric acid coating is present (**Table 9**). Here, the major products are the same for both kaolinite, silica, and alumina, but while kaolinite forms only limonene glycol, alumina has only 82.4% glycol. Adding the reactivity in these two tables also shows a great disparity between the kinetics on alumina and silica as compared to kaolinite. Comparison of the reactive uptake for each of these oxides showed that they were only 11-21% as reactive as kaolinite without acid, and only 13-27% with acid coating. It is clear that flawed logic has led to the addition of

alumina and silica reactivity and these two mineral surfaces cannot compare to clays.

Table 8: Products greater than 10% on each type of dust in reactions without nitric acid and the kinetics of each reaction. % kaolinite reactivity was calculated by dividing the reactive uptake coefficient of each reaction with the uptake coefficient for kaolinite. Glycol was the major product for all reactions besides gamma alumina. Only illite reacted faster than kaolinite, and both alumina phases had less than 20% of the reactivity of kaolinite.

	Terpineol	Carveol	Limonene-Glycol	Reactive Uptake (γ)	% Kaolinite Reactivity
α Al ₂ O ₃		31.77%	44.95%	1.09E-09	19%
γ Al ₂ O ₃		53.25%	17.07%	0.65E-09	11%
SiO ₂			97.49%	1.26E-09	21%
Kaolinite			99.60%	5.89E-09	100%
Montmorillonite	13.32%	19.25%	54.74%	1.57E-09	27%
Illite			92.70%	19.2E-09	326%
Arizona Test Dust			91.43%	0.13E-09	2%

Figure 9: Products greater than 10% on each type of dust in reactions with nitric acid coating and the kinetics of each reaction. % kaolinite reactivity was calculated by dividing the reactive uptake coefficient of each reaction with the uptake coefficient for kaolinite. Glycol was the major product for all reactions besides on montmorillonite. Alumina still reacted significantly slower than kaolinite.

	Terpineol	Limonene-Glycol	Terpin	Reactive Uptake (γ)	% Kaolinite Reactivity
α Al ₂ O ₃		82.41%		11.3E-09	31%
γ Al ₂ O ₃		82.42%		4.60E-09	13%
SiO ₂	16.50%	70.17%		9.95E-09	27%
Kaolinite		100.00%		36.6E-09	100%
Montmorillonite			91.18%	25.6E-09	70%
Arizona Test Dust		91.00%		1.05E-09	3%

The combination of large size and low reactive uptake coefficient on Al₂O₃ makes it surprising that so many heterogeneous reaction models would base their reactions off of an alumina surface or any of the other large oxides. Most studied dust storms do not even contain aluminum atoms alone in particles that are transported long distances, and pure particles in general are rare with aluminosilicates and mixed particles dominating storm composition⁹. SiO₂ (quartz) occurs in high abundance, though, likely due to the small particle small size and ease of erosion⁴⁴, thus it may be considered an exception to the general lack of pure particles and makes this oxide relevant. Again, particles with large diameters are not observed to travel

long distances due to their weight or air resistance, and they settle out of clouds quickly^{8,15}. The effects of nitric acid may have also been widely misrepresented in literature due to the oxide-favored model of most heterogeneous reaction research. The effects of a nitric acid coating on mineral surfaces increase the relevance of clays due to more impactful size decreases to increase atmospheric lifetime. Additionally, combined with the smaller relative size decrease on aluminum oxides, the kinetic effects of acid are more pronounced on these surfaces. Uptake speed, size, and products of reactions on mineral surfaces may not be reliably represented in literature because of the prevalence of a model that relied on adding the reactivity of oxides to equal aluminosilicate clays. When studying the atmosphere, we need to use a more complete model of the dust composition that includes clays and actual dust samples because dust storms are more than just purified elemental oxides.

In terms of our actual dust sample, Arizona Test Dust did not show similarity to the pure oxides tested in this study, but it had an unknown composition and very different particle size. Based on this difference, it is not surprising that the pure oxides were so different in kinetics and product distributing. It is clear that $\text{SiO}_2 + \text{Al}_2\text{O}_3$ is not the same as an aluminosilicate clay or an actual dust sample, as we originally predicted. Additionally, though we assume that it likely has a high quartz and calcite content, we do not know what type of quartz crystals are present and the calcite we originally tested was unreactive. It is likely that there are further clays contained within this sample, but without specific identification of which types of particles are present, it is difficult to estimate the reactivity. Additionally, due to moisture in the sample when it was received, it was heated at $\sim 150^\circ\text{C}$ for 48 hours to evaporate any water prior to reaction, but dust heating can change the surface structure and surface sites available, so heating the sample may have changed the reactivity. There are a large number of

unknowns with this dust sample, but due to the fact that it shows little to no similarity to the pure aluminum oxides, it further supports movement away from the oxide-based model.

5.2 Recommendations for Ongoing Research

Going forward, research on the study of trace gases reacting on mineral surfaces needs to include more diverse surfaces. By including clays or other particles that are actually measured in dust storms we may have more success in predicting the amount of SOA formed each year. This information would allow us to truly understand the impacts of our VOC pollution and historical climate events and move forward with suggestions on improving air quality. While the EPA currently has measures in place to limit some VOC pollution²⁷, the limits they set could be updated to include the larger scale pollution outside of consumer products. Additionally, recognition of the effects of SOA for visibility and health could be expanded upon and brought into the Clean Air Act to tighten regulation and further remove pollutants from the air. Researching more clays or looking at more diverse and complex samples of real dust storms would allow us to track the progress of reactions as storms move, and thus understand the locations most affected by reactions of VOCs on mineral surfaces. Stepping away from the $\text{Al}_2\text{O}_3 + \text{SiO}_2 = \text{clay}$ model will allow actual representations of the impacts and radiative forcing effects due to reactions on mineral surfaces.

To improve modeling, we can also improve techniques to identify the specific surfaces found in atmospheric samples. While approximate composition can be estimated from elemental abundance and ratios, the actual reactive sites are difficult to probe and identify. Computer modeling studies coupled with experimental reactions could improve the reliability and likelihood of hypothesized mechanisms.

Within these reactions, more work is needed on aluminosilicate clays and other clays

commonly identified in storms. This study was limited to three clays and three oxides and was mainly a comparison to dust from the southwestern US, but composition of this sample varies widely from other deserts and storm sources globally. For example, our sample of Arizona Test Dust likely contains much less kaolinite and illite than samples from the Sahara or Gobi Desert, thus using these different samples would yield very different results for reactivity¹³. Also, there are other oxides actually identified including iron-oxide, which causes the red rains in the Mediterranean⁷, so a comprehensive model is needed to understand the locational variability in reactivity and decrease the error and unknown nature of mineral dust effects in the atmosphere. Studying a greater number of trace gases would likely improve the relevance of the study as the data would be more widely applicable to different regions with a different profile of VOCs. The most abundant VOC, isoprene, merits significant study due to its high levels of emission each year, and its derivative monoterpenes are so wide in range that a number of products and reactions need to be identified.

Within the scope of our research, time limitations did not allow for duplicate measurements of the products and reactive uptakes on different dusts. In addition, a complete set of reactions with nitric acid could not be finished on all of the clays. In the future I hope that this lab is able to complete these reactions and publish the data so that improvements of current models can be made. Recalculation of uptake coefficients in literature might provide new insights for sinks and lifetimes of different species that currently do not match up with atmospheric measurements. All in all, I would hope that increased usage of aluminosilicate clays might replace pure aluminum oxides as model surfaces because clays are significantly more atmospherically and reactively relevant.

Bibliography

- (1) Gazit, C. *Surviving the Dust Bowl*; PBS, 2007.
- (2) Cook, B. I.; Miller, R. L.; Seager, R. *Proc. Natl. Acad. Sci. U. S. A.* **2009**, *106* (13), 4997–5001.
- (3) Carbon Offset Research & Education. Radiative Forcing
<http://www.co2offsetresearch.org/aviation/RF.html> (accessed Mar 8, 2016).
- (4) Usher, C. R.; Michel, A. E.; Grassian, V. H. *Chem. Rev.* **2003**, *103* (12), 4883–4939.
- (5) IPCC. *Climate Change 2014: Synthesis Report. Contribution of Working Groups I, II and III to the Fifth Assessment Report of the Intergovernmental Panel on Climate Change*; 2014.
- (6) EPA. *Inventory of U.S. Greenhouse Gas Emissions and Sinks: 1990-2011 – Trends (Chapter 2: Trends in Greenhouse Gas Emissions)*; 2013.
- (7) Avila, A.; Queralt-Mitjans, I.; Alarcón, M. *J. Geophys. Res.* **1997**, *102* (D18), 21977.
- (8) Blanco, A.; de Tomasi, F.; Filippo, E.; Manno, D.; Perrone, M. R.; Serra, R.; Tafuro, a. M.; Tepore, A. *Atmos. Chem. Phys. Discuss.* **2003**, *3* (5), 4633–4670.
- (9) Caquineau, S.; Gaudichet, A.; Gomes, L.; Legrand, M. *J. Geophys. Res.* **2002**, *107* (D15, 4251), 10.1029/2000JD000247.
- (10) Karydis, V. A.; Kumar, P.; Barahona, D.; Sokolik, I. N.; Nenes, A. *J. Geophys. Res. Atmos.* **2011**, *116* (D23), D23204.
- (11) Woodill, L. a.; O’Neill, E. M.; Hinrichs, R. Z. *J. Phys. Chem. A* **2013**, *117* (27), 5620–5631.
- (12) Pitter, R. L.; Pruppacher, H. R. *Quart. J. R. Met. Soc.* **1973**, *99* (421), 540–550.
- (13) Claquin, T.; Schulz, M.; Balkanski, Y. *J. Journal of Geophysical Research.* 1999, p 22243.
- (14) Wedepohl, K. *Geochim. Cosmochim. Acta* **1995**, *59* (7), 1217–1232.
- (15) Geng, H.; Hwang, H.; Liu, X.; Dong, S.; Ro, C.-U. *Atmos. Chem. Phys.* **2014**, *14* (7), 3307–3323.
- (16) Busca, G. In *Metal Oxides*; 2005; pp 247–318.
- (17) Liu, Q.; Zhang, Y.; Liu, Y.; Zhang, M. *Environ. Sci. Pollut. Res. Int.* **2014**, *21* (15), 9325–9333.
- (18) Tazi, S.; Rotenberg, B.; Salanne, M.; Sprik, M.; Sulpizi, M. *Geochim. Cosmochim. Acta* **2012**, *94*, 1–11.
- (19) Umann, B.; Arnold, F.; Schaal, C.; Hanke, M.; Uecker, J.; Aufmhoff, H.; Balkanski, Y.; Van Dingenen, R. *J. Geophys. Res. Atmos.* **2005**, *110* (22), 1–17.
- (20) Sokolik, I. N.; Winker, D. M.; Bergametti, G.; Gillette, D. a.; Carmichael, G.; Kaufman, Y. J.; Gomes, L.; Schuetz, L.; Penner, J. E. *J. Geophys. Res.* **2001**, *106*

- (D16), 18015.
- (21) Tang, Y.; Carmichael, G. R.; Kurata, G.; Uno, I.; Weber, R. J.; Song, C. H.; Guttikunda, S. K.; Woo, J. H.; Streets, D. G.; Wei, C.; Clarke, A. D.; Huebert, B.; Anderson, T. L. *J. Geophys. Res. D Atmos.* **2004**, *109* (19), 1–21.
 - (22) Jokinen, T.; Berndt, T.; Makkonen, R.; Kerminen, V.-M.; Junninen, H.; Paasonen, P.; Stratmann, F.; Herrmann, H.; Guenther, A. B.; Worsnop, D. R.; Kulmala, M.; Ehn, M.; Sipilä, M. *Proc. Natl. Acad. Sci. U. S. A.* **2015**, *112* (23), 7123–7128.
 - (23) Allaby, M. *Fog, Smog, and Poisoned Rain*; Infobase Publishing, 2014.
 - (24) US National Park Service. Environmental Factors - Great Smoky Mountains National Park <http://www.nps.gov/grsm/learn/nature/environmentalfactors.htm> (accessed Mar 8, 2016).
 - (25) Rasmussen, R. A.; Went, F. W. *Proc. Natl. Acad. Sci. U. S. A.* **1965**, *53* (1), 215–220.
 - (26) Kang, D.; Aneja, V. P.; Zika, R. G.; Farmer, C.; Ray, J. D. *J. Geophys. Res.* **2001**, *106* (D3), 3133.
 - (27) EPA. *Clean Air Act - As Amended Through P.L. 108-201*; 2004.
 - (28) EPA, C. *Ozone and Health*; Sacramento, CA, 2015.
 - (29) Maksymiuk, C. S.; Gayahtri, C.; Gil, R. R.; Donahue, N. M. *Phys. Chem. Chem. Phys.* **2009**, *11* (36), 7810–7818.
 - (30) Fuentes, J. D.; Lerdau, M.; Atkinson, R.; Baldocchi, D.; Bottenheim, J. W.; Ciccioli, P.; Lamb, B.; Geron, C.; Gu, L.; Guenther, a.; Sharkey, T. D.; Stockwell, W. *Bull. Am. Meteorol. Soc.* **2000**, *81* (7), 1537–1575.
 - (31) Leungsakul, S.; Jaoui, M.; Kamens, R. M. *Environ. Sci. Technol.* **2005**, *39* (24), 9583–9594.
 - (32) Kesselmeier, J.; Staudt, M. *J. Atmos. Chem.* **1999**, *33* (1), 23–88.
 - (33) Tanner, R. L.; Parkhurst, W. J. *J. Air Waste Manage. Assoc.* **2000**, *50* (8), 1299–1307.
 - (34) Kroll, J. H.; Seinfeld, J. H. *Atmos. Environ.* **2008**, *42* (16), 3593–3624.
 - (35) Staniec, A. *Acid Catalyzed Heterogeneous Reaction of Limonene with Mineral Aerosols: A New Mechanism for The Organic Coating of Inorganic Aerosols*, Drew University, 2015.
 - (36) O'Neill, E. M.; Kawam, A. Z.; Van Ry, D. A.; Hinrichs, R. Z. *Atmos. Chem. Phys.* **2014**, *14*, 47–60.
 - (37) Angelini, M. M.; Garrard, R. J.; Rosen, S. J.; Hinrichs, R. Z. *J. Phys. Chem. A* **2007**, *111* (17), 3326–3335.
 - (38) Reddy, B. In *Metal Oxides: Chemistry and Applications*; J. L. G. Fierro, Ed.; CRC Press: Boca Raton, FL, 2005; pp 215–246.
 - (39) Surratt, J. D.; Chan, A. W. H.; Eddingsaas, N. C.; Chan, M.; Loza, C. L.; Kwan, A. J.; Hersey, S. P.; Flagan, R. C.; Wennberg, P. O.; Seinfeld, J. H. *Proc. Natl. Acad. Sci. U.*

- S. A.* **2010**, *107* (15), 6640–6645.
- (40) Liu, X.; Cheng, J.; Sprik, M.; Lu, X.; Wang, R. *Geochim. Cosmochim. Acta* **2015**, *168*, 293–301.
- (41) Sulpizi, M.; Gageot, M. P.; Sprik, M. *J. Chem. Theory Comput.* **2012**, *8* (3), 1037–1047.
- (42) Gageot, M.-P.; Sprik, M.; Sulpizi, M. *J. Phys. Condens. Matter* **2012**, *24* (12), 124106.
- (43) Mlinar, A. N.; Zimmerman, P. M.; Celik, F. E.; Head-Gordon, M.; Bell, A. T. *J. Catal.* **2012**, *288*, 65–73.
- (44) Ro, C. U.; Kim, H.; Oh, K. Y.; Yea, S. K.; Lee, C. B.; Jang, M.; Van Grieken, R. *Environ. Sci. Technol.* **2002**, *36* (22), 4770–4776.